Design of Control Strategies for Low Voltage DC Residential Grids

Guilherme Marto Paraíso

Thesis to obtain the Master of Science Degree in

Electrical and Computer Engineering

Supervisors: Prof. José Fernando Alves da Silva
Prof. Sónia Maria Nunes dos Santos Paulo Ferreira Pinto

Examination Committee

Chairperson: Prof. Rui Manuel Gameiro de Castro
Supervisor: Prof. Sónia Maria Nunes dos Santos Paulo Ferreira Pinto
Member of the Committee: Prof. Victor Manuel de Carvalho Fernão Pires

November 2018

Declaration

I declare that this document is an original work of my own authorship and that it fulfills all the requirements of the Code of Conduct and Good Practices of the Universidade de Lisboa.

Acknowledgements

First, I would like to thank my supervisors Prof. J. Fernando Silva and Prof. Sónia Pinto, who showed an interest in working with me long before this thesis started. Without their guidance and insight, I would not have been able to accomplish this work.

I would also like to thank my friends and colleagues at Instituto Superior Técnico, that accompanied me throughout these five years, for their friendship. I also thank all my friends from Leiria who have supported me during this period of my life.

Furthermore, I would like to thank my family especially my parents and my brother for their patience and support. They have provided me with everything I needed to become a better student and have been always by my side when I needed.

Finally, I would like to thank Instituto de Engenharia de Sistemas e Computadores – Investigação e Desenvolvimento of Universidade de Lisboa (INESC-ID/IST/ULisboa) for granting me a scholarship within project UID/CEC/50021/2013 of Fundação para a Ciência e Tecnologia (FCT).

Resumo

Nos últimos anos verificou-se um aumento no interesse acerca das redes de distribuição DC de forma a substituir ou complementar as antigas redes de distribuição AC.

Uma micro-rede DC é composta por múltiplas fontes e cargas interconectadas através de conversores e filtros de entrada. Algumas dessas cargas são cargas de potência constante que podem causar instabilidade na rede devido à sua característica não linear.

O objetivo desta tese é desenhar um uma rede de distribuição DC constituída por uma fonte de energia DC e um conversor redutor. Este conversor redutor tem de ser capaz de controlar e regular a tensão no barramento DC após a conexão destas cargas de potência constante. Para isso foram dimensionados 2 sistemas de controlo não linear.

O primeiro controlador proposto é uma combinação de duas técnicas de controlo não-linear baseadas na Teoria de estabilidade de Lyapunov e chama-se *Backstepping Sliding Mode Controller* (BSMC). O segundo sistema de controlo utiliza apenas a técnica de controlo não-linear *Backstepping* e é denominada *Recursive Backstepping Controller* (RBC). Com estes novos controladores não-lineares pretende-se reduzir significativamente (mais de 50 vezes) o valor da capacidade do condensador do conversor principal.

Para servir como referência, controladores lineares foram também desenhados e aplicados ao mesmo sistema de modo a poder comparar controladores que se baseiam em teoria de controlo linear e não linear.

Estas 3 estratégias de controlo são então comparadas em termos de sobretensões/subtensões e resposta a transitórios. Simulações e resultados obtidos experimentalmente confirmam o melhor desempenho do BSMC que se baseia na teoria de controlo não linear.

Palavras chave: Micro-rede DC, Conversor DC-DC Redutor, Controladores Lineares, Controladores Não-lineares, Backstepping Control, Sliding Mode Control

Abstract

In recent years there has been an increasing in interest in DC distribution networks to replace or complement the traditional AC distribution networks.

A DC micro-grid consists of multiple sources and loads interconnected through converters and input filters. Some of these loads are constant power loads (CPL) that may cause instability in the grid due to its non-linear characteristic.

The purpose of this thesis is to design a DC distribution grid consisting of a DC power source and a Buck converter. This converter must be able to control and regulate the voltage on the DC bus after the connection of these CPLs. In order to do so, 2 non-linear control systems were designed.

The first proposed controller is a combination of two non-linear control techniques based on the Lyapunov Stability Theory and is called Backstepping Sliding Mode Controller (BSMC). The second control system uses only the non-linear Backstepping control technique and is called Recursive Backstepping Controller (RBC). With these novel non-linear controllers, it is aimed to reduce significantly (more than 50 times) the value of the main converter capacitor value.

To serve as reference, linear controllers were also designed and applied to the same system in order to compare controllers that are based on linear and non-linear control theory.

These 3 control strategies are then compared in terms of overvoltages / undervoltages and transient responses. Simulations and results obtained experimentally confirm the best performance is obtained with BSMC which is based on nonlinear control theory.

Keywords: DC Microgrid, Buck Converter, Linear Controllers, Non-Linear Controllers, Backstepping Control, Sliding Mode Control

Table of Contents

List of Figures

List of Tables

List of Acronyms

AC	Alternating Current
BSMC	Backstepping Sliding Mode Controller
CPL	Constant Power Loads
DC	Direct Current
ESS	Energy Storage System
IGBT	Insulated-gate Bipolar Transistor
PI	Proportional-Integral
PWM	Pulse Width Modulation
RBC	Recursive Backstepping Controller
RE	Renewable Energy
SMC	Sliding Mode Control

List of Symbols

Latin Symbols

a_i	Gain margin of the current PI controller
a_v	Gain margin of the voltage PI controller
b_k	Polynomial coefficients
C	Main converter capacitor
C_{f*}	Load input filter capacitor
C_*	Load converter capacitor
c_i	Backstepping control gain
D	Open subset of $\mathbb{R}^n$
d	Line length
e_x	Control error of variable x
f	Switching frequency
f_*	Load converter switching frequency
I_0	Output current (Grid current)
i_D	Diode current
i_L	Inductor current
i_{Lref}	Inductor reference current
i_S	Supply Current
i_{Lv}	Inductor virtual current
K_D	Modulator incremental gain
K_E	Modulator static gain
K_i	Integration coefficient of the current PI controller
K_{iV}	Integration coefficient of the voltage PI controller
K_p	Proportional gain of the current PI controller
K_{pV}	Proportional gain of the voltage PI controller
k_i	Backstepping current control gain
k_I	Backstepping integral control gain
k_v	Backstepping voltage control gain
k_W	Anti-Windup feedback gain
L	Main converter inductance
L_{f*}	Loads input filter inductor
L_*	Load converter inductor
P_0	Output Power
P_{0*}	Load Output Power
R	Resistor
R_{0*}	Load resistance
r_c	Capacitor parasitic resistance
r_{cf*}	Parasitic resistances of the loads input filter capacitor
r_i	Negative incremental resistance
r_l	Inductor parasitic resistance
r_{lf*}	Parasitic resistances of the loads input filter inductor
r_p	Damping resistors of the loads input filters
S	Main converter IGBT
s	Sliding surface
t	Time
T	Period
T_d	Average value of t_d
t_d	Delay time
T_p	Time constant of the pole of the current PI controller
T_{pv}	Time constant of the pole of the voltage PI controller
T_z	Time constant of the zero of the current PI controller
T_{zv}	Time constant of the zero of the voltage PI controller
U	Input Voltage
u	Control input

u_c	Modulating signal
$u_{cmáx}$	Upper limit of the modulating signal
V_*	Lyapunov function
V_0	Output voltage (Grid voltage)
V_{0i}	Load Output voltage
V_{0ref}	Output reference voltage
v_c	Capacitor voltage
v_{cref}	Capacitor reference voltage
v_L	Inductor voltage
v_R	Resistor voltage
W	Total energy stored on a capacitor
W_*	Positive definite function
x	System state vector
x_e	Equilibrium point
x_{ref}	Reference waveform
z	Tracking error

Greek Symbols

α_i	Current Sensor Gain
α_V	Voltage Sensor Gain
γ	Buck converter mode of operation
Δ	Bandwidth
Δi_L	Current ripple
ΔV_0	Voltage ripple
δ	Duty-cycle
$\bar{\delta}$	Duty-cycle average value
η	Efficiency
ξ	Damping ratio
τ	Time constant
Φ_*	Strictly positive constant

Chapter 1

Introduction

1.1 Background

In the late 19th Century there was a big dispute about how should electric power be transmitted known as “war of currents”. On one side Nikola Tesla and George Westinghouse argued that Alternating Current (AC) was the best way to distribute power and on the other side Thomas Edison claimed that Direct Current (DC) system was the superior and safest choice for electric power distribution. Eventually, AC won this battle mainly because after the invention of the transformer it was easy to convert the voltage to higher or lower levels and also due to the lower cost of implementation. However, DC systems did not disappear entirely and, in fact in California, San Francisco there is still a 250 Volt DC power system that feeds DC power to some historical buildings [1].

In recent years with the advancement in semiconductor technology that allowed to step-up or step-down DC voltage, DC networks are a possible solution to replace or complement the traditional AC distribution system [2]. These DC grids may become an important asset to integrate Renewable Energy (RE) such as photovoltaic, which intrinsically produce DC. With the penetration of these RE sources arises the need for distributed power systems to be equipped with Energy Storage Systems (ESSs) capable of compensating the differences between generated and consumed power. Therefore, DC microgrids have an advantage because it is easier to integrate these ESSs, as most of them require the connection to DC [3].

Most of the household appliances as: laptops, TV’s, tablets, phones and newer lighting systems use DC power. DC power can be also used in heating, air conditioners and refrigeration. Supplying these loads through the conventional AC distribution network requires additional DC-AC conversion stages [4], with the consequent power losses. However, with a DC system the number of conversion stages would be reduced which will, therefore, decrease the cost of implementation and leading to a higher efficiency.

One of the main challenges for DC distribution grids is to deal with the interaction between power electronic loads which may lead to stability issues. These loads can be divided in three groups: constant current loads that draw a fixed current value; constant voltage loads that maintains the value of the voltage constant regardless of the current; and constant power loads (CPL). The first two types include resistive loads, heating equipment, inductive loads, LED lamps [5] and do not

represent a significant problem to the grid. However, CPLs will have a great impact on the stability and robustness of the DC microgrid due to its negative impedance characteristic [6] [7] [8].

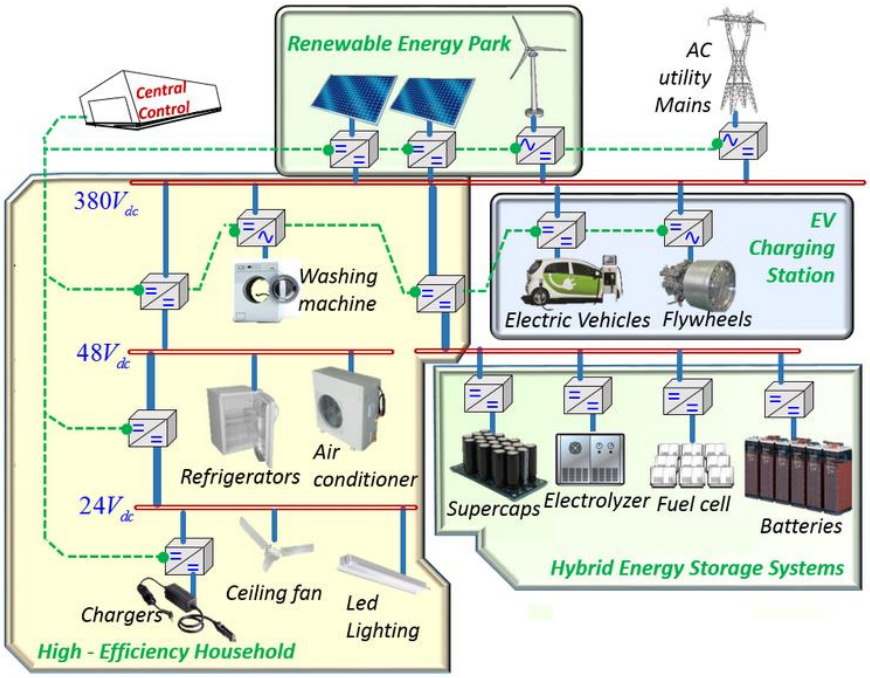

Fig. 1.1 – Low voltage residential DC microgrid (modified from [9])

Several methods have been proposed to control microgrids and to counteract instabilities caused by CPLs. Among them are, passivity-based control, which uses passive elements to dampen the oscillations of the system, active damping [5], a solution that involves a modification in the control loop by creating a damping effect of passive damping or modifying the DC bus capacitance. Many nonlinear control methods have also been applied to overcome this problem such as, feedback linearization [10], where a nonlinear model of the system is linearized by defining appropriate state-variables, sliding mode controllers [11] operating at a variable frequency to guarantee that the variables to control can track a certain reference path.

1.2 Thesis Objectives

The main aim of this dissertation is to further investigate control methodologies for DC microgrids. To achieve that objective, a DC microgrid, composed of a main DC-DC converter and a DC power source, with multiple connected CPLs is designed. The objective is to design non-linear and linear controllers for the main converter and assess how they behave in possible operation scenarios where non-linear loads are connected or disconnected to/from the grid. These controllers should guarantee the stability of the grid by maintaining the DC grid voltage at a constant value or bounded by pre-set limits.

By using non-linear controllers, it is intended to drastically reduce the capacitance value of the main converter capacitor to a value around 50 times lower. This will allow a technologic leap, using film capacitors instead of state-of-art electrolytic capacitors whose average lifespan is short. Additionally, it will reduce the short-circuit currents, which will depend directly on the main capacitor value.

Simulations will be carried out with MATLAB/Simulink for both linear and non-linear control approaches, and the results obtained with the different control models are then compared. On a smaller scale, experimental verification will also be a part of this work.

1.3 Thesis Organization

This dissertation is divided into six more chapters.

A model for the whole DC grid is designed in chapter 2. It is seen how CLPs connected to DC residential grids may represent a problem to the stability of the grid. Then the main DC-DC converter is introduced and modified to improve the grid's stability.

In chapter 3, the objective is to present Lyapunov stability theory and use it in the analysis and design of nonlinear systems. Two nonlinear techniques are introduced: Sliding Mode Control and Backstepping Control.

In chapter 4, the theory explained in the previous chapter is applied in the context of this work and two nonlinear controllers are proposed for the main DC-DC converter: Backstepping Sliding Mode Controller and Recursive Backstepping Controller.

In chapter 5, linear PI controllers are designed for the main DC-DC converter and are used as a reference for comparison.

Chapter 6 presents the results using these 3 control approaches. The last chapter presents the conclusions that can be drawn from this dissertation as well as ideas to possible future work that could be done.

Chapter 2

Modelling the DC Distribution Grid

The DC Distribution grid will be modelled using a main DC-DC converter to guarantee the DC voltage level in the grid. The loads will be modelled as constant power loads

2.1 DC Microgrid Configuration

For the purpose of this study, the DC distribution grid is considered to be fed from a DC power source (e.g. a renewable energy system with storage). The DC power supply then supplies the grid main DC-DC buck converter. This power converter will be used to control the DC grid voltage V_o and limit the short-circuit current by acting on the switching transistor duty-cycle.

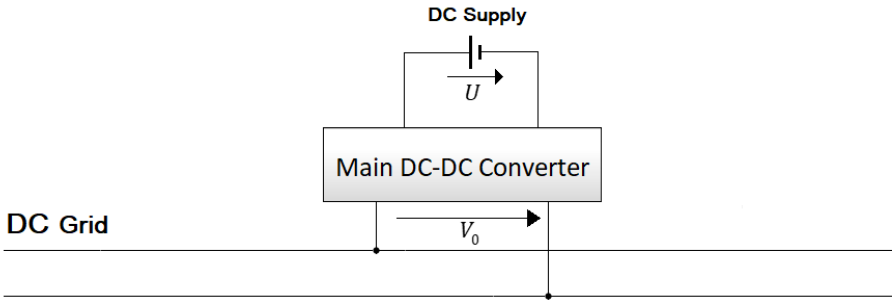

Fig. 2.1 – DC grid representation

The characteristic loads of this grid will be mainly other power converters feeding loads, such as computers, screens set, phones, that can be considered to absorb a constant power at a given operating point, due to the relatively small switching periods of the power converters. Therefore, the load converters operate at constant power, and in steady-state, at constant number of loads the main converter will be operated at constant power ($dP_0 = 0$), which means that:

$$P_0 = V_0 I_0 = constant \tag{2.1}$$

This behaviour may be regarded as a negative incremental resistance ri [12], that can be defined as:

$$dP_0 = V_0 dI_0 + I_0 dV_0 = 0 \Leftrightarrow \frac{V_0}{I_0} = -\frac{dV_0}{dI_0} = r_i \tag{2.2}$$

Therefore, if the voltage across the capacitor increases/decreases, the current that flows through the load will decrease/increase respectively. As shown in Fig. 2.2 the voltage is inversely proportional to the current.

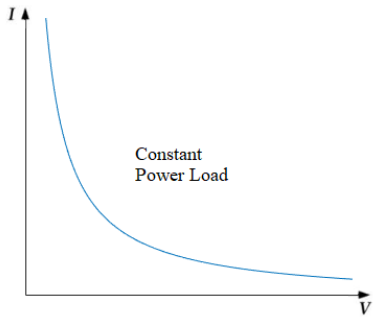

Fig. 2.2 -V-I curve of Constant Power Load

Different loads will be connected to the DC bus through different lines with negligible losses. Each load is often a Buck converter with its own output power. Each buck converter has an input filter which is represented in Fig. 2.3.

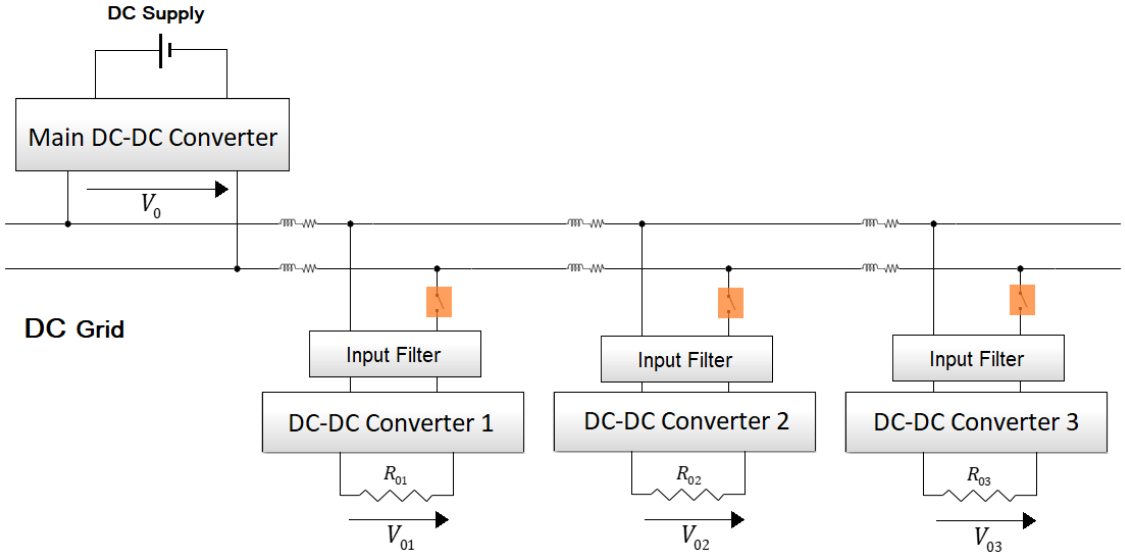

Fig. 2.3 – DC grid and Load representation

These input filters are necessary to avoid the converter switching current pulses from being reflected back into the line, attenuating the switching harmonics from the line present in the converter input current [13].

2.2 Step-Down Converter - Main Converter

The Step-Down converter (also called Buck converter) is a type of a DC-DC power converter, that decreases the DC voltage from a higher value at the input into a lower value at the output, using a switching IGBT, a diode, an inductor and a capacitor. The topology is represented in Fig. 2.4.

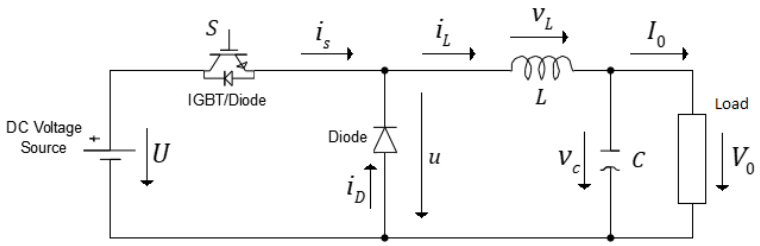

Fig. 2.4 – Main DC-DC Buck converter

In the continuous conduction [14] mode when the switching transistor is driven ON, the diode is reversed biased and is OFF, the current flows through the inductor as well as the load and the capacitor. At the same time, the inductor is storing some energy coming from the power supply. When the switching transistor is driven OFF, the energy stored in the inductor as well as the energy in the capacitor helps feed the load, as the diode becomes forward biased and guarantees a path to the i_L current.

Due to the high frequency semiconductor switching, the output voltage will not be exactly constant, it will present ripple ΔV_0 that should be negligible. Fig. 2.5 shows the most relevant waveforms obtained for a Buck converter.

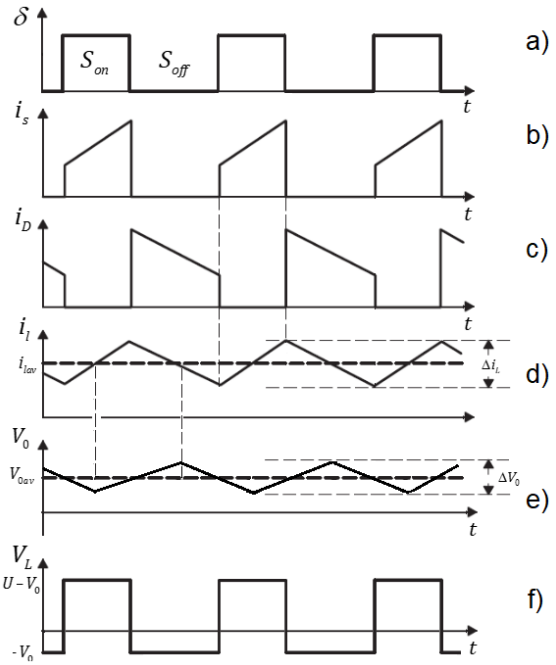

Fig. 2.5 – Buck Converter waveforms of a) semiconductor driving voltage; b) supply current; c) diode current; d) inductor current; e) output voltage f) inductor's voltage

2.3 Ideal LC Filter

DC-DC converters operating at constant power P_{OUT}, with an efficiency η, will be connected to the DC microgrid. Fig. 2.6 represents the output filtering stage of the main DC/DC converter.

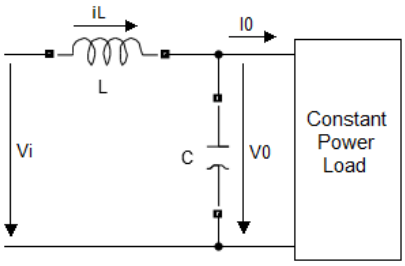

Fig. 2.6 – Main DC/DC ideal LC Filter

The dynamical behaviour of the output filter capacitor voltage V_0 will be described by the set of linear equations:

$$\begin{cases} C\dfrac{dV_0}{dt} = i_L - I_0 \\ L\dfrac{di_L}{dt} = V_i - V_0 \end{cases} \tag{2.3}$$

Calculating the time derivative of the first equation and using the second equation of (2.3) to simplify the result, it is obtained the following equation which unveils an incremental negative resistance:

$$C\frac{d^2V_0}{dt^2} + \left(-\frac{P_{OUT}}{\eta V_0^2}\right)\frac{dV_0}{dt} + \left(\frac{1}{L}\right)V_0 - \frac{V_i}{L} = 0 \tag{2.4}$$

From (2.4), the term $-\dfrac{P_{OUT}}{\eta V_0^2}$ includes the efficiency η of the converter feeding the constant power load P_{OUT}, and represents an incremental negative conductance. The correspondent negative resistance r_i may also be defined as:

$$r_i = \frac{dV_0}{dI_0} = \frac{d}{dI_0}\left(\frac{P_{OUT}}{I_0}\right) = -\frac{P_{OUT}}{\eta I_0^2} = -\eta\frac{V_0^2}{P_{OUT}} \tag{2.5}$$

The transfer function of the DC-DC converter filter can be obtained, and is seen to be dependent on the incremental negative resistance r_i:

$$\frac{V_0(s)}{V_i(s)} = \frac{\dfrac{1}{LC}}{s^2 + s\dfrac{1}{r_i C} + \dfrac{1}{CL}} \tag{2.6}$$

The system dynamics can be examined by plotting the roots of the transfer function and see how they change with the variation of the output power which will therefore change the negative resistance r_i (the resistance is positive for negative variations of P_{OUT}):

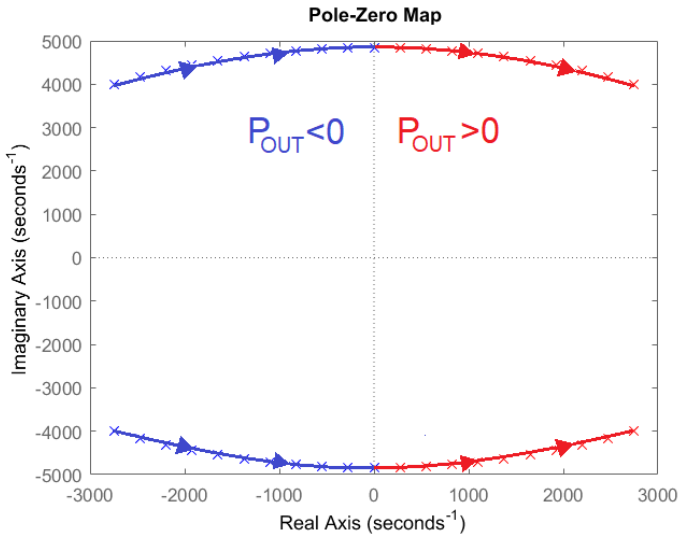

Fig. 2.7 – Pole-zero map of the ideal LC filter with a Constant Power Load

Fig. 2.7 shows that as the output power variation changes from negative to positive, the location of the two conjugated poles move from the left half part of the complex plane, which corresponds to negative values of output power P_{OUT} variation (positive r_i), to the right half of the complex plane, which corresponds to positive values of output power P_{OUT} (negative r_i), leading to system instability.

2.4 LC filter considering the effect of the parasitic resistors

In the previous section, the parasitic resistors of the main converter output filter inductance and capacitance were not included in the analysis. However, to do a more realistic analysis on the dynamic performance of the converter, these parasitic resistances should be considered, since they can be used for damping, even though they introduce extra losses and filtering degradation.

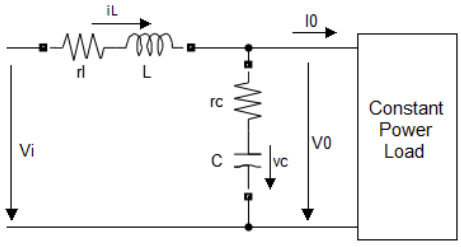

Fig. 2.8 – LC filter with parasitic resistors

From Fig. 2.8, the derivative of the capacitor voltage can be obtained from (2.7), where r_c represents the intrinsic resistor of capacitor C and r_i represents the intrinsic resistor of inductance L.

$$i_L - I_0 = C\frac{dv_c}{dt} \Leftrightarrow i_L - I_0 = C_f\frac{dV_0}{dt} - Cr_c\frac{di_L}{dt} + Cr_c\frac{dI_0}{dt} \tag{2.7}$$

Knowing that $I_0 = \frac{P_{OUT}}{\eta V_0} \Rightarrow \frac{dI_0}{dt} = -\frac{P_{OUT}}{\eta V_0^2}\frac{dV_0}{dt}$ it is possible to rewrite i_L as a function of V_0:

$$= V_0\left(\frac{P_{OUT}L + Cr_cV_0^2}{V_0^2(L - Cr_cr_l)}\right) + \frac{dV_0}{dt}\left(\frac{L(V_0^2C - P_{OUT}Cr_c)}{V_0^2(L - Cr_cr_l)}\right) - \frac{Cr_cV_i}{L - Cr_cr_l} \tag{2.8}$$

Applying Laplace transformation to (2.7) and (2.8), and using the result obtained in (2.8) in equation (2.7), after a few simplifications it is possible to obtain the transfer function:

$$\frac{V_0(s)}{V_i(s)} = \frac{s\frac{r_cr_i}{L(r_i + r_c)} + \frac{r_i}{LC(r_i + r_c)}}{s^2 + s\left(\frac{1}{Cr_c} - \frac{L - Cr_cr_l}{r_cLC} + \frac{-L + Cr_cr_i}{LC(r_i + r_c)}\right) + \frac{r_i - r_l}{LC(r_i + r_c)}} \tag{2.9}$$

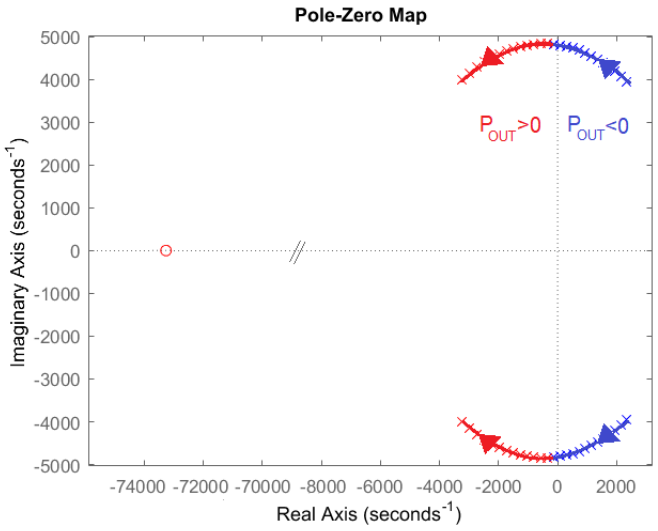

Fig. 2.9 – Pole-zero map of the damped LC filter with a Constant Power Load

Fig. 2.9 shows that instability can still occur. Stability can be achieved increasing the filtering capacitor (at the expense of a poor lifetime of the unavoidable electrolytic capacitors [15]) or increasing losses in damping resistors. Alternatively, closed-loop advanced non-linear controllers can be designed with a fast-dynamic response.

Chapter 3

Lyapunov's Stability and non-linear control

The objective of this chapter is to present an important tool for analysing nonlinear control systems. One of the most important properties when studying a dynamic system is to assess whether the system is stable or not. Different techniques are available, but perhaps one the most useful and general approaches is the second method of Lyapunov (also called Lyapunov's direct method) proposed in 1892 by the Russian Mathematician, Aleksandr Mikhailovich Lyapunov.

3.1 Fundamental Definitions

Consider a nonlinear system described by the following differential equations

$$\frac{dx}{dt} = \dot{x} = f(x) \tag{3.1}$$

Where $f(x)$ is an nx1 nonlinear continuously differentiable function, x is the nx1 state vector and n is the order of the system. An equilibrium condition exists if all the variables, have such values $x_{1e}, \ldots, x_{ne}$ that all the derivatives $dx_1/dt, \ldots, dx_n/dt$ are simultaneously zero. Assuming that x_e is an equilibrium point of $f(x)$ and that this point corresponds to the origin (i.e. x_e=0). In the sense of Lyapunov, stability means solutions that start near an equilibrium point x_e and remain near x_e forever.

3.1.1 Stability Theorems

The equilibrium point can be characterized as stable, unstable or asymptotically stable in the following conditions [16]:

Stable: The equilibrium point x=0 of the system (3.1) is said to be stable at t_0 if, for a given $\Psi > 0$, there is a $\psi=\psi(\Psi, t_0)>0$:

$$\|x(t_0)\| < \psi \Rightarrow \|x(t)\| < \Psi \quad \forall t \geq t_0 > 0 \tag{3.2}$$

Unstable: if it is not stable

In many applications, it is useful to know if the system will return to the equilibrium point after infinite time, following any slight disturbance.

Asymptotically stable: The equilibrium point x=0 is asymptotically stable if the system is stable and there is a ψ>0 such that

$$\|x(t_0)\| < \psi \Rightarrow \lim_{t\to\infty} x(t) = 0 \tag{3.3}$$

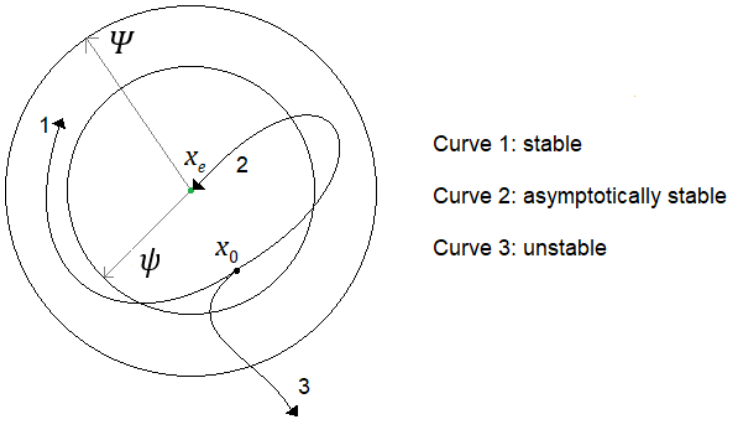

Fig. 3.1 – Concepts of stability

3.1.2 Lyapunov functions

Considering a function V: $D \to \mathbb{R}$, a scalar function $V(x)$, and assuming that $V(x)$ is continuous and has continuous partial derivatives for to all of its arguments.

V is said to be positive semi-definite in D if:

- $V(0) = 0$
- $V(x) \geq 0 \qquad \forall x \neq 0 \, , x \in D$

(3.4)

V is said to be positive definite in D if:

- $V(0) = 0$
- $V(x) > 0 \qquad \forall x \neq 0 \, , x \in D$

(3.5)

V is said to be negative semi-definite in D if:

- $V(0) = 0$
- $V(x) \leq 0 \qquad \forall x \neq 0 \, , x \in D$

(3.6)

V is said to be negative definite in D if:

- $V(0) = 0$
- $V(x) < 0 \qquad \forall x \neq 0 \, , x \in D$

(3.7)

A continuously differentiable scalar function V is called a Lyapunov function of (3.1) if satisfies (3.5) and (3.8):

$$\dot{V}(x) \leq 0 \qquad \forall x \in D \tag{3.8}$$

3.1.3 Lyapunov's Second method

Having defined stability and asymptotic stability of equilibrium points and Lyapunov functions, our goal now is to find ways to determine stability.

Lyapunov's second method is related to the concept of energy stored in a physical system. If the system is asymptotically stable, the stored energy decays with time. A simple example to illustrate this is an RC circuit, where the voltage source is removed at *t*=0s and the fully charged capacitor C discharges through the resistor R.

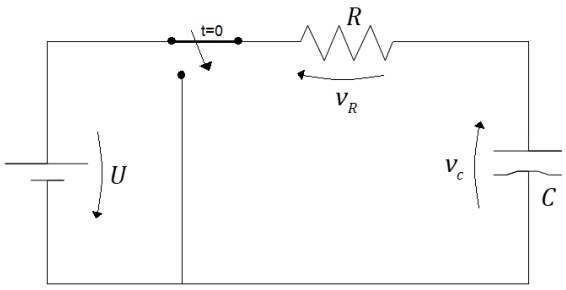

Fig. 3.2 – Example for an RC series circuit

$$C\frac{dv_c}{dt} + \frac{v_c}{R} = 0 \tag{3.9}$$

The solution to this differential equation is:

$$v_c(t) = Ue^{-\frac{t}{RC}} \tag{3.10}$$

The instantaneous energy stored in the capacitor is given by:

$$W(v_c) = \frac{1}{2}Cv_c^2 = \frac{1}{2}C\left(Ue^{-\frac{t}{RC}}\right)^2 \tag{3.11}$$

By inspecting the equation above, it can be seen that $W(u_C)$ is positive definite. The time-derivative of (3.11), which is always negative, is:

$$\frac{dW}{dt} = \dot{W} = -\frac{1}{R}U^2e^{-\frac{2t}{RC}} \tag{3.12}$$

So, according to Lyapunov's second method the equilibrium point $v_C = 0$, is asymptotically stable, as expected. This concept of energy is replaced with a more general concept called Lyapunov function.

The objective of this section is to formalize and generalize the previous example. Let x=0 be an equilibrium point for (3.1) and $D \subset \mathbb{R}^n$ be a domain containing x=0. Let V: $D \to \mathbb{R}$ be a continuously differentiable function such that:

$$\begin{aligned} &V(0) = 0 \\ &V(x) > 0 \ \ in \ \ D - \{0\} \\ &\dot{V}(x) \leq 0 \ \ in \ \ D \end{aligned} \tag{3.13}$$

Then x=0 is *stable*. Moreover, if

$$\dot{V}(x) < 0 \ \ in \ \ D - \{0\} \tag{3.14}$$

Then x=0 is *asymptotically stable*, that is, the asymptotic stability is achieved if conditions in (3.13) are adjusted to require $\dot{V}(x)$ to be negative definite instead of semi definite.

The above statements are applied to the local analysis of stability. To assess global asymptotic stability of a system an additional condition on function V must be satisfied, $V(x)$ must be radially unbounded:

$$V(x) \to 0 \qquad \|x\| \to \infty \tag{3.15}$$

Then x=0 is *global asymptotically stable* if*:*

- $V(0) = 0$
- $V(x) > 0 \ \ in \ \ D - \{0\}$
- $\dot{V}(x) \leq 0 \ \ in \ \ D$
- $V(x) \to 0 \qquad \|x\| \to \infty$

(3.16)

3.2 Sliding Mode Control

Sliding Mode Control (SMC) is a robust nonlinear method for control of linear and non-linear systems developed in the early 1960's [17]. The principle of SMC is to apply different feedback controllers acting on the opposite sides of a predetermined surface (sliding surface) in the system space. Each controller makes the system trajectory to converge towards the sliding surface. Once this region is reached, it remains on it thereafter.

Consider a nonlinear system with the following mathematical form:

$$\dot{x} = f(x,t) + g(x,t)u(t) \tag{3.17}$$

Where $x \in \mathbb{R}^n$ is the state vector, $u \in \mathbb{R}$ is the control input, $f(x,t)$ and $g(x,t)$ $\mathbb{R}^n$ are nonlinear functions. The control objective is to force the output to track a reference signal x_{ref} or more

specifically the error associated with this variable, $e_x = x_{ref} - x$, to tend to some small vicinity of zero.

SMC design is a two-step procedure. The first step involves determining the sliding surface in accordance with the control objective, so that the desired system dynamics are achieved during sliding mode. The second step is concerned with the design of a discontinuous control law capable of forcing the system state to reach this surface in finite-time.

Step 1: Introducing a new scalar function of the system state it is often defined by a set of relationships between state error variables of the system [18].

$$s(x) = \phi_1 e_x + \phi_2 \dot{e}_x + ... + \phi_r e_x^{(r-1)} \tag{3.18}$$

Where $\phi_1, \ldots, \phi_n$ are strictly positive constants, and the integer r is the relative degree between x_{ref} and u. In order to achieve asymptotic convergence of the state variables (i.e. $\lim_{t\to\infty} e_x, ..., e_x^{(r-1)} = 0$), the function $s(x)$ must be driven to zero in finite time. From a geometric perspective $s(x)=0$ defines a surface in the error space called sliding surface (or sliding manifold). Consequently, the dynamics of the reduced system is given by the following differential equation:

$$\phi_1 e_x + \phi_2 \dot{e}_x + ... + \phi_n e_x^{(r-1)} = 0 \tag{3.19}$$

For the sake of simplicity, we will consider a first-order system $r=2$.

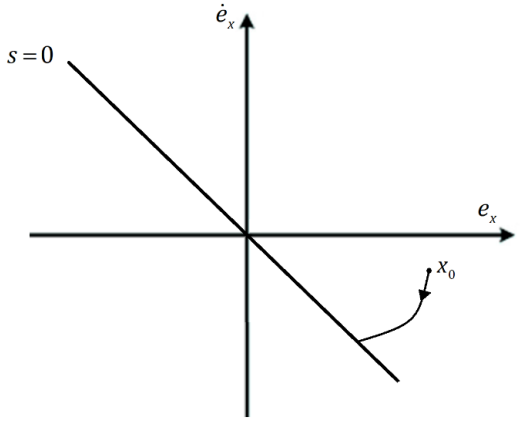

Fig. 3.3 – Ideal sliding motion

Step 2: The controller u should be able to steer the system trajectories onto the sliding manifold, and achieve $s(x)=0$ in finite time. This task can be accomplished by applying Lyapunov's direct method to the s-dynamics. Consider the following candidate Lyapunov function

$$V(s) = \frac{1}{2} s^2 \tag{3.20}$$

To fulfil all the requirements in (3.16), its derivative of (3.20) should satisfy the condition:

$$\dot{V}(s) = s\dot{s} < 0 \tag{3.21}$$

The time derivative of $s(x)$ is given by:

$$\begin{aligned}\dot{s}(x) &= \phi_1(\dot{x}_{ref} - \dot{x}) \\ &= \phi_1\left(\dot{x}_{ref} - f(x,t) - g(x,t)u\right)\end{aligned} \tag{3.22}$$

It can be seen that the control action, appears in the equation above and it is from that equation that u will be designed in order to achieve $s\dot{s} < 0$. In general, u can be generalized in the following form:

$$u = \begin{cases} u^+ & if \quad s(x) > 0 \\ u^- & if \quad s(x) < 0 \end{cases} \tag{3.23}$$

Or

$$u = \begin{cases} u^+ & if \quad s(x) > 0 \ \& \ \dot{s}(x) < 0 \\ u^- & if \quad s(x) < 0 \ \& \ \dot{s}(x) > 0 \end{cases} \tag{3.24}$$

Real Sliding motion

Ideally the control signal u should be able to switch at an infinite frequency and force the system trajectory to slide along the manifold as shown in Fig. 3.3. However, in real-life applications, the controller can only switch at a finite frequency, due to unmodeled dynamics, delays of the actuating and measuring devices and to the presence of noise and/or disturbances. This may lead to low control accuracy, high losses in electric circuits and high wear of moving mechanical parts. This problem can be solved by substituting the controller on (3.23) by a hysteresis comparator with a bandwidth of Δ. The control law will be given by:

$$u = \begin{cases} u^+ & if \quad s(x) > \Delta \\ u^- & if \quad s(x) < -\Delta \end{cases} \tag{3.25}$$

This bandwidth will limit the switching frequency and set a region in space where the state trajectories will be bounded as shown in Fig. 3.4.

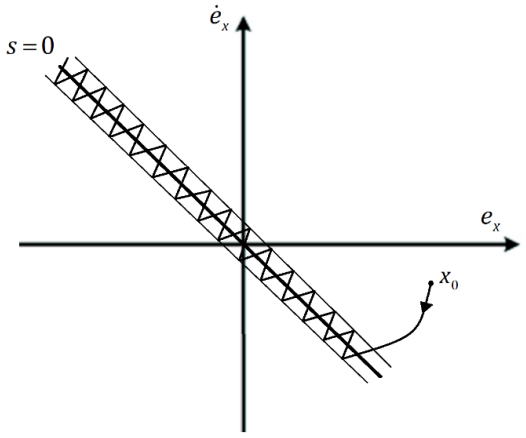

Fig. 3.4 – Real sliding mode trajectory within a boundary layer Δ

3.3 Backstepping Controller Design

Backstepping is a nonlinear control design technique, developed by Peter V. Kokotovic in the 1990's [19]. The main idea behind backstepping is to break down the non-linear system into smaller subsystems and use some of the state variables as "virtual controls" to obtain intermediate control laws by making use of Lyapunov functions [20] . This technique can be applied to non-linear systems which have a strict feedback form (3.26).

$$\begin{aligned}\dot{x}_1 &= f_1(x_1) + g_1(x_1)x_2 \\ \dot{x}_2 &= f_2(x_1, x_2) + g_2(x_1, x_2)x_3 \\ &\vdots \\ \dot{x}_n &= f_n(x_1, x_2, \ldots, x_{n-1}, x_n) + g_n(x_1, x_2, \ldots, x_{n-1}, x_n)u\end{aligned} \tag{3.26}$$

where $(x_1, x_2, \ldots, x_n) \in \mathbb{R}^n$ are the system states, $u \in \mathbb{R}$ is the control input and $g_i(x_1, x_2, \ldots, x_n) \neq 0$ for $1 < i < n$. Our goal is to track a signal reference signal x_{1ref} with the state x_1. To illustrate the backstepping procedure, we begin by examining with the simplest example, for which n=2. This tracking problem ($x_1 \rightarrow x_{1ref}$) can be converted into a regulation problem by defining the tracking error variable z_1.

$$z_1 = x_{1ref} - x_1 \tag{3.27}$$

Rewriting $\dot{x}_1$ in terms of this new variable z_1:

$$\dot{z}_1 = \dot{x}_{1ref} - f_1(x_1) - g_1(x_1)x_2 \tag{3.28}$$

Then x_2 is regarded as the virtual control input for the system in (3.28) and its desired value denoted as x_{2ref}, this value can be chosen so that the $\dot{z}_1$-subsystem is asymptotically stable. Consider the following candidate Lyapunov function for (3.28):

$$V_1(z_1) = \frac{1}{2}z_1^2 \tag{3.29}$$

A standard quadratic function, positive definite and radially unbounded with derivative:

$$\dot{V}_1(z_1) = z_1\dot{z}_1 \tag{3.30}$$

Substituting $\dot{z}_1$ in the equation above by (3.28):

$$\dot{V}_1(z_1) = z_1\left(\dot{x}_{1ref} - f_1(x_1) - g_1(x_1)x_2\right) \tag{3.31}$$

A new state is introduced which represents the difference between the virtual control x_2 and x_{2ref}.

$$z_2 = x_{2ref} - x_2 \tag{3.32}$$

Equation (3.31) is then written in terms of this new variable, resulting in:

$$\dot{V}_1(z_1) = z_1\left(\dot{x}_{1ref} - f_1(x_1) - g_1(x_1)\left(x_{2ref} - z_2\right)\right) \tag{3.33}$$

In order to make (3.33) negative definite:

$$\frac{\partial V}{\partial z_1}\frac{\partial z_1}{\partial t} \leq -W_1(x) < 0, \qquad \forall x \in \mathbb{R}^n \tag{3.34}$$

Where $W_1(x)$ is a positive definite continuous function chosen as $W_1(x) = c_1 z_1^2$ where c_1 is higher than 0. Then through equation (3.33) and (3.34) the first intermediate control law is obtained:

$$x_{2ref} = \frac{1}{g_1(x_1)}\left(z_1 c_1 - f_1(x_1) + \dot{x}_{1ref}\right), \qquad c_1 > 0 \tag{3.35}$$

Then this choice of intermediate control gives:

$$\dot{V}_1(z_1) = z_1\left(-z_1 c_1 + z_2\right) = -c_1 z_1^2 + g_1(x_1) z_1 z_2 \tag{3.36}$$

If we are able to make this second error $z_2 \rightarrow 0$ for $t \rightarrow \infty$ then we will also make the first error variable $z_1 \rightarrow 0$ for $t \rightarrow \infty$. Hence the cross term $g_1(x_1)z_1z_2$ will be 0 and $\dot{V}_1$ becomes negative definite and according to Lyapunov's stability z_1 is asymptotically stable. To ensure that the actual value of x_{2ref} follows the desired value, the Lyapunov function is augmented with a quadratic term as follows:

$$V_2 = V_1 + \frac{1}{2} z_2^2 \tag{3.37}$$

In this final step the final control law for the control variable u, that appears in the expression for $\dot{z}_2$, is designed:

$$\dot{z}_2 = \dot{x}_{2ref} - \dot{x}_2 = \dot{x}_{2ref} - f_2(x_1, x_2) - g_2(x_1, x_2)u \tag{3.38}$$

Taking the time derivative of V_2 results in:

$$\begin{aligned} \dot{V}_2(z_1, z_2) &= \dot{V}_1(z_1) + z_2\left(\dot{x}_{2ref} - f_2(x_1, x_2) - g_2(x_1, x_2)u\right) \\ &= -c_1 z_1^2 + g_1(x_1) z_1 z_2 + z_2\left(\dot{x}_{2ref} - f_2(x_1, x_2) - g_2(x_1, x_2)u\right) \end{aligned} \tag{3.39}$$

The equation above can be made negative definite using the same approach as in (3.34) and defining a new positive definite function $W_2(x)$:

$$W_2(x) = c_1 z_1^2 + c_2 z_2^2, \qquad c_{1,2} > 0 \tag{3.40}$$

By selecting the following control law:

$$u = \frac{1}{g_2(x_1, x_2)}\left(z_2 c_2 - f_2(x_1, x_2) + g_1(x_1) z_1 + \dot{x}_{2ref}\right) \tag{3.41}$$

The derivative of the Lyapunov function V_2 is negative definite and according to Lyapunov's second method the control goal is achieved and the equilibrium z_1 =0 z_2 =0 is globally asymptotically stable.

3.3.1 Generalization to Higher Order Systems

The goal is to track the value x_{1ref} with x_1. The design process starts at the known stable system and recursively 'back out' new controllers that progressively stabilize each other subsystem. The process terminates when the final external control (u) is reached. First by defining the tracking error variables:

$$z_i = x_{iref} - x_i, \qquad i = 1,2,\ldots,n \tag{3.42}$$

The system in (3.26) can be rewritten in terms of these new variables:

$$\begin{aligned} \dot{z}_1 &= \dot{x}_{1ref} - f_1(x_1) - g_1(x_1)x_2 \\ \dot{z}_2 &= \dot{x}_{2ref} - f_2(x_1,x_2) - g_2(x_1,x_2)x_3 \\ &\vdots \\ \dot{z}_n &= \dot{x}_{nref} - f_n(x_1,x_2,\ldots,x_{n-1},x_n) - g_n(x_1,x_2,\ldots,x_{n-1},x_n)u \end{aligned} \tag{3.43}$$

Then for each sub-system, a candidate Lyapunov function is derived:

$$V_i = V_{i-1} + \frac{1}{2}z_i^2 \tag{3.44}$$

Taking the time derivative of (3.44):

$$\dot{V}_i = \dot{V}_{i-1} + z_i\dot{z}_i \tag{3.45}$$

To ensure that $\dot{V}_i < 0$, a positive definite function W_i is defined as:

$$W_i = W_{i-1} + c_i z_i^2, \qquad c_i > 0, \qquad i = 1,\ldots,n \tag{3.46}$$

By matching equation (3.45) with (3.46) , the virtual control laws are given by:

$$\begin{aligned} x_{2ref} &= \frac{1}{g_1}\left(z_1c_1 - f_1 + \dot{x}_{1ref}\right) \qquad c_1 > 0 \\ x_{iref} &= \frac{1}{g_i}\left(z_ic_i - f_i + g_{i-1}z_{i-1} + \dot{x}_{iref}\right), \qquad c_i > 0, \qquad i = 2,\ldots,n \\ u &= x_{nref} \end{aligned} \tag{3.47}$$

Choosing the control laws above, the derivatives of V_i will be negative definite. According to Lyapunov Stability criteria, this implies that the equilibrium point z_1 =0, z_2 =0, ..., z_n =0 is globally asymptotically stable ($x_1 \to x_{1ref}$ for $t \to \infty$).

Chapter 4

Non-Linear Controllers for Buck DC-DC Converters

Most physical systems are nonlinear, including DC-DC converters. Their control design represents a major difficulty. Classic control methods are based on Taylor-series-linearized system dynamics in conjunction with linear control techniques. However, they are likely to fail under large deviations from its equilibrium point. Hence in this chapter, two non-linear design controllers are presented to control the DC grid main DC-DC converter based on Lyapunov's second method for stability at constant power loads. In section 4.1, the concept is to force the state variable to reach a sliding manifold in finite time and to stay on the manifold [16]. In section 4.2, the idea is to break a design problem for the full system into a sequence of design problems for low order subsystems and recursively use some states as "virtual controls" to obtain the intermediate control laws with the Lyapunov functions [20] [21].

4.1 Backstepping Sliding Mode Controller

This control approach combines Backstepping and Sliding Mode Control (BSMC): the voltage controller (outer loop), that will define the inductor's current i_{Lref} needed to follow a reference voltage (V_0=V_{0ref}) using Backstepping theory; and the current controller (inner loop), which is based in Sliding Mode Control, to force the current tracking behaviour ($i_L = i_{Lref}$).

4.1.1 Backstepping Voltage controller

4.1.1.1 Voltage controller without integral action

The average model of the buck converter represented in Fig. 2.4 can be written as

$$\begin{cases} \dot{v}_C = \dfrac{i_L - I_0}{C} \\ \dot{i}_L = \dfrac{u - v_C}{L} \end{cases} \tag{4.1}$$

If the control objective is to guarantee:

$$v_c = v_{c_{ref}} \tag{4.2}$$

Then the error or deviation between the reference voltage and the voltage across the capacitor may be defined as:

$$e_{v_C} = v_{c_{ref}} - v_c \tag{4.3}$$

Considering the following Lyapunov function:

$$V_L = \frac{e_{v_C}^2}{2} \tag{4.4}$$

As discussed in the previous section, the Lyapunov function must be positive definite:

$$V_L > 0 \quad \forall e_{v_C} \neq 0 \tag{4.5}$$

And V_L must be radially unbounded to ensure global asymptotic stability:

$$V_L \to \infty \ \ for \ \ \|t\| \to \infty \tag{4.6}$$

Its time derivative must be negative definite. In order to guarantee $\dot{V}_L < 0$, k_v in equation (4.7) must be greater than zero:

$$\dot{V}_L = e_{v_C} \frac{de_{v_C}}{dt} = -k_v e_{v_C}^2 \tag{4.7}$$

Since all the requirements are met, the 2nd method for global asymptotic stability can now be applied:

$$V_L = \frac{e_{v_C}^2}{2} \Rightarrow \frac{dV_L}{dt} < 0 \Rightarrow e_{v_C} \frac{de_{v_C}}{dt} < 0 \Rightarrow \frac{de_{v_C}}{dt} = -k_v e_{v_C} \tag{4.8}$$

Calculating de_{vC}/dt by the use of equation (4.1) and (4.3):

$$\frac{de_{v_C}}{dt} = \frac{dv_{Cref}}{dt} - \frac{i_L - I_0}{C} \tag{4.9}$$

Using the stability condition (4.8) in the equation above and replacing i_L for i_{Lref}, where i_{Lref} is the virtual control variable, returns the inductor's current i_{Lref} needed to follow the reference voltage (V_0=V_{0ref}):

$$\frac{dv_{Cref}}{dt} - \frac{i_{Lref} - I_0}{C} = -k_v e_{v_C} \Leftrightarrow i_{Lref} = Ck_v e_{v_C} + C\frac{dv_{Cref}}{dt} + I_0 \tag{4.10}$$

Fig. 4.1 represents the diagram block used to implement the non-linear Backstepping voltage controller.

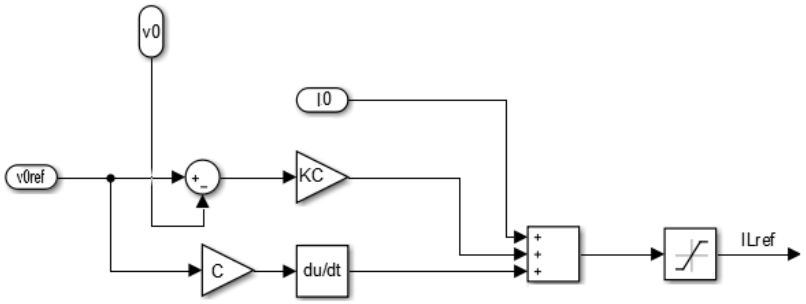

Fig. 4.1 – Non-linear voltage controller

From (4.10) a non-linear voltage controller is obtained that will generate the signal i_{Lref} to be used in the current controller.

4.1.1.2 Voltage controller with integral action

To guarantee zero static error that may occur due to parameter mismatch or measuring errors in (4.10), one possible solution is to extend the previous procedure and add the integral of the error e_{vC} in the Lyapunov function while ensuring that it is 0. By defining a new Lyapunov function:

$$V_{L1} = k_I \frac{e_I^2}{2} + \frac{e_{vC}^2}{2}, \qquad k_I > 0 \tag{4.11}$$

Where e_I is defined as:

$$e_I = \int_0^t e_{vC} dt = 0 \tag{4.12}$$

The procedure is similar to the one previously used: the time derivative of V_{L1} is obtained:

$$\frac{dV_{L1}}{dt} = k_I e_I \frac{de_I}{dt} + e_{vC} \frac{de_{vC}}{dt} = k_I e_I e_{vC} + e_{vC} \frac{de_{vC}}{dt} \tag{4.13}$$

To ensure asymptotically stability, then it is required:

$$\frac{dV_{L1}}{dt} < 0 \Rightarrow k_I e_I e_{vC} + e_{vC} \frac{de_{vC}}{dt} = -k_v e_{vC}^2 \tag{4.14}$$

After some algebraic manipulation of equation (4.14) and considering (4.9), the virtual control action is now given by:

$$i_{Lref} = C\left(k_v e_{vC} + k_I e_I + \frac{dv_{Cref}}{dt} \right) + I_0 \tag{4.15}$$

4.1.2 Sliding Mode Current Controller

Having described the Sliding Mode procedure in section 3.2, here it is applied in the context of this work to generate the driving signal for the semiconductor for the main converter. Let us consider a function γ defined to characterize the converter operation in Fig. 2.4:

$$\gamma = \begin{cases} 1 & Semiconductor\ is\ ON\ \ (S\ ON) \\ 0 & Semiconductor\ is\ OFF\ \ (S\ OFF) \end{cases}$$

If $\gamma = 1$ $\quad v_L = U - V_0 = L\frac{di_L}{dt} > 0 \quad ,U > V_0$ (4.16)

If $\gamma = 0$ $\quad v_L = -V_0 = L\frac{di_L}{dt} < 0 \quad ,U > V_0$ (4.17)

By inspection it is possible to rewrite the two equations above in one equation:

$$v_L = L\frac{di_L}{dt} = \gamma u - V_0 \tag{4.18}$$

The current controller objective is to make $i_L = i_{Lref}$, meaning that the error associated with this objective is $e_{iL} = i_{Lref} - i_L$. For control design a time-varying linear surface $s(x)$ is defined as follows:

$$s(i_L) = i_{Lref} - i_L = e_{iL} \tag{4.19}$$

The Lyapunov's direct method is used as a stable condition to guarantee that the sliding surface is reached after a finite period of time. By defining the Lyapunov function:

$$V_{L2} = \frac{1}{2}s^2 = \frac{e_{i_L}^2}{2} \tag{4.20}$$

The stability condition is satisfied, if $s\dot{s} < 0$. This means that:

If $e_{i_L} > 0$ then, $\frac{de_{i_L}}{dt} < 0 \Rightarrow \frac{di_L}{dt} > \frac{di_{Lref}}{dt}$ (4.21)

If $e_{i_L} < 0$ then, $\frac{de_{i_L}}{dt} > 0 \Rightarrow \frac{di_L}{dt} < \frac{di_{Lref}}{dt}$ (4.22)

Ideally, to achieve a zero error, between the reference value and the variables to control, an infinite switching frequency would be required. However, due to the physical limitations of semiconductors, this is not possible. So, the error must be bounded by $-\Delta/2 < e_{iL} < +\Delta/2$ and the control action to do so is:

If $e_{iL} > +\frac{\Delta}{2} \Rightarrow i_{Lref} > i_L$ then, $i_L \uparrow \Rightarrow \frac{di_L}{dt} > \frac{di_{Lref}}{dt} \Rightarrow S\,ON\ (\gamma = 1)$ (4.23)

If $e_{iL} < -\frac{\Delta}{2} \Rightarrow i_{Lref} < i_L$ then, $i_L \downarrow \Rightarrow \frac{di_L}{dt} < \frac{di_{Lref}}{dt} \Rightarrow S\,OFF\ (\gamma = 0)$ (4.24)

From equation (4.16) and (4.17) it is clear in order to guarantee that $di_L/dt > di_{Lref}/dt$, then the semiconductor S must be ON. On the other hand, if $di_L/dt < di_{Lref}/dt$ then the semiconductor S must be OFF. In other words, when the inductance current is more than the upper current reference, the power switch is turned off and when the inductance current is less than the lower current reference, the power switch is turned on.

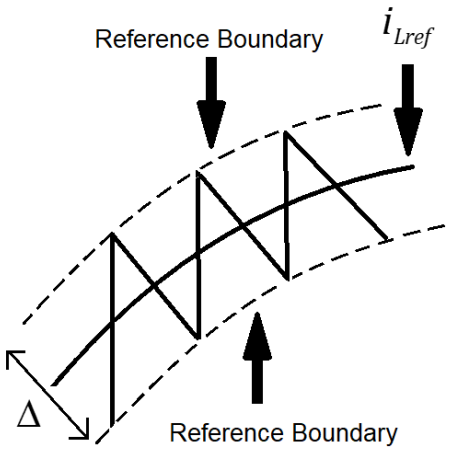

Fig. 4.2 – Actual sliding motion

$$\gamma = \begin{cases} 1 & if \quad e_{iL} > +\Delta/2 \\ 0 & if \quad e_{iL} < -\Delta/2 \end{cases} \tag{4.25}$$

The signal to drive the semiconductor S is obtained using a hysteresis comparator. This controller is able to provide a fast-dynamic response, is stable and robust to load variations or any type of dynamic perturbations.

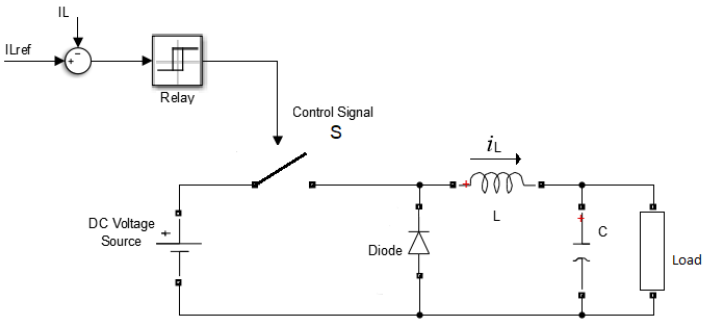

Fig. 4.3 Non-linear current controller and buck converter representation

4.2 Recursive Backstepping Controller

The first step to design the Recursive Backstepping Controller (RBC) is to derive a virtual control input i_{Lv} to minimize the tracking error of the output voltage e_{vC}=v_{Cref} - v_C. The result is the same as the one presented in section 4.1.1.1.

$$i_{Lv} = Ck_v e_{v_C} + C\frac{dv_{Cref}}{dt} + I_0 \tag{4.26}$$

In the second step, to obtain the input control u input that enforces the i_L virtual control input (i_L= i_{Lv}), recursively apply the above method by defining the error of the virtual control input:

$$e_{iL} = i_{Lv} - i_L \tag{4.27}$$

Applying the 2nd method of Lyapunov stability, by proposing a candidate Lyapunov function positive definite:

$$V_{L3} = \frac{e_{vC}^2}{2} + \frac{e_{iL}^2}{2} \tag{4.28}$$

To make sure that the time derivative of (4.28) is negative:

$$\frac{dV_{L3}}{dt} = e_{vC}\frac{de_{vC}}{dt} + e_{iL}\frac{de_{iL}}{dt} < 0 \Rightarrow e_{vC}\frac{de_{vC}}{dt} + e_{iL}\frac{de_{iL}}{dt} = -k_v e_{vC}^2 - k_i e_{iL}^2 \tag{4.29}$$

Using (4.3) and (4.1), and replacing $i_L = i_{Lv} - e_{iL}$, then equation (4.29) can be rewritten as:

$$e_{vC}\left(\frac{dv_{Cref}}{dt} - \frac{i_{Lv} + e_{iL} - I_o}{C}\right) + e_{iL}\left[\frac{di_{Lv}}{dt} - \frac{u - v_C}{L}\right] = -k_v e_{vC}^2 - k_i e_{iL}^2 \tag{4.30}$$

From (4.29) and (4.30), the output voltage error times its derivative can be rewritten and simplified. Then, using the result of (4.8), it is possible to obtain:

$$\begin{aligned} & e_{vC}\frac{de_{vC}}{dt} = e_{vC}\left(\frac{dv_{Cref}}{dt} - \frac{i_{Lv} + e_{iL} - I_o}{C}\right) \Leftrightarrow \\ \Leftrightarrow & \frac{de_{vC}}{dt} = \left(\frac{dv_{Cref}}{dt} - \frac{i_{Lv} - I_o}{C}\right) + \frac{e_{iL}}{C} \Leftrightarrow \\ \Leftrightarrow & \frac{de_{vC}}{dt} = -k_v e_{vC} + \frac{e_{iL}}{C} \end{aligned} \tag{4.31}$$

Thus:

$$e_{vC}\left(-k_v e_{vC}\right) + e_{iL}\left[\frac{di_{Lv}}{dt} + \frac{e_{vC}}{C} - \frac{u - v_C}{L}\right] = -k_v e_{vC}^2 - k_i e_{iL}^2 \tag{4.32}$$

Considering (4.26) and (4.32) and $i_L = i_{Lv} - e_{iL}$, the term di_{Lv}/dt is given as:

$$\frac{di_{Lv}}{dt} = Ck_v\frac{de_{vC}}{dt} + \frac{dI_o}{dt} + C\frac{d^2v_{Cref}}{dt^2} = Ck_v\left(\frac{dv_{Cref}}{dt} - \frac{i_{Lv} - e_{iL} - I_o}{C}\right) + \frac{di_o}{dt} + C\frac{d^2v_{Cref}}{dt^2} \tag{4.33}$$

Replace this value of di_{Lv}/dt in the square brackets of (4.32):

$$e_{iL}\left[Ck_v\left(\frac{dv_{Cref}}{dt} - \frac{i_{Lv} - e_{iL} - I_o}{C}\right) + \frac{di_o}{dt} + C\frac{d^2v_{Cref}}{dt^2} + \frac{e_{vC}}{C} - \frac{u - v_C}{L}\right] = -k_i e_{iL}^2 \tag{4.34}$$

After some manipulations the control input u is obtained:

$$u = e_{vC}\left(\frac{L}{C} - LCk_v^2\right) + e_{iL}L\left(k_v + k_i\right) + L\frac{dI_o}{dt} + LC\frac{d^2v_{Cref}}{dt^2} + v_C \tag{4.35}$$

From this control input average value u, the duty-cycle average value $\bar{\delta}$, which is the control signal (Fig. 4.4) for the buck converter, can be obtained from $u = \bar{\delta}U$.

$$\bar{\delta} = \frac{1}{U}\left(e_{vC}\left(\frac{L}{C} - LCk_v^2 \right) + e_{iL}L\left(k_v + k_i\right) + L\frac{dI_o}{dt} + LC\frac{d^2 v_{Cref}}{dt^2} + v_C \right) \tag{4.36}$$

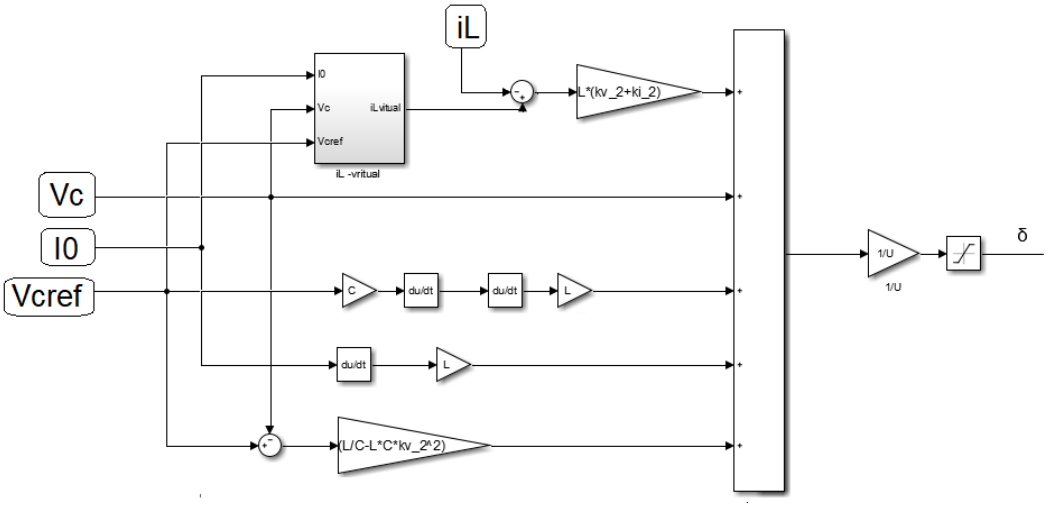

Fig. 4.4 – MATLAB/Simulink model of the Recursive Backstepping Controller

The average value of the duty cycle $\bar{\delta}$ is then applied to a linear modulator that will generate the driving signal for the semiconductor S for the main converter transistor (Fig. 2.4).

Chapter 5

Linear Controllers for Buck DC-DC Converters

Linear Controllers for non-linear power converters are used in many applications [18]. They are mostly seen in industry to regulate flow, temperature, pressure and many other industrial process variables [22]. In this section, a Proportional-Integral (PI) current and voltage controllers are designed for the main DC-DC converter. PI controllers eliminate the residual steady state error resulting from pure P controllers, they are very popular due to its suitability, simple structure, easy to design and low cost. The basic concept of a closed loop control system for a switching power converter is shown in Fig. 5.1.

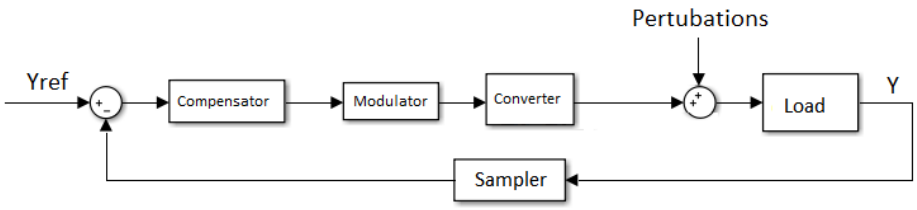

Fig. 5.1 - Block diagram of a commutated processor with a converter in operation

The modulator applies the driving signal to the semiconductor. To do this a comparison is made between a modulating signal u_c and a periodic waveform called carrier signal at frequency equal to the switching frequency. Without any perturbations the modulator guarantees a correct behaviour in steady state regime. However, in a dynamic regime this behaviour may become erratic and any deviation compared to reality will create an error leading to harmonics. The carrier signal is a saw-tooth waveform, $r(t)$, with maximum amplitude u_{cmax} and period T.

$$r(t) = \frac{u_{cmáx} t}{T} \tag{5.1}$$

The modulator compares the modulating signal u_c with $r(t)$, turning the semiconductor OFF when $r(t)$ exceeds u_c, defining the conduction interval that finishes when:

$$r(t = \delta T) = u_c = \frac{u_{cmáx} \delta T}{T} \tag{5.2}$$

From here results in a duty cycle δ:

$$\delta = \frac{u_c}{u_{c\max}} \tag{5.3}$$

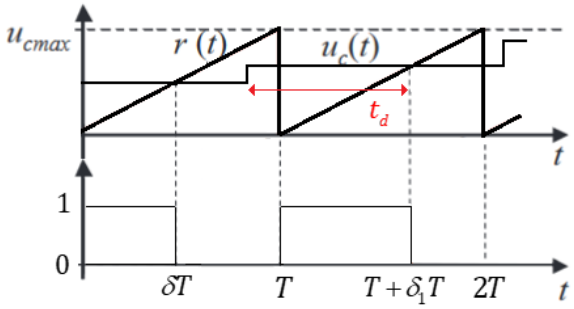

Fig. 5.2 - Saw-tooth Modulator (modified from [14])

In a switching converter, the duty cycle is defined in every period and can only be modified in the next period. This means that after the definition of δ the signal u_c may change causing a delay t_d. It is reasonable to consider for the delay the mean value T_d of the random variable t_d:

$$T_d = \frac{T}{2} \tag{5.4}$$

Assuming that this modulator is going to be applied in a Buck converter the relationship between the output voltage and the input voltage is:

$$V_p = \delta U = u_C \frac{U}{u_{cmax}} \tag{5.5}$$

The static gain from this modulator associated with this converter is $K_E = V_p / u_c$ [14], and has the same value as the incremental gain:

$$K_D = \frac{V_p}{u_C} = \frac{U}{u_{Cmax}} \tag{5.6}$$

The transfer function of the association Modulator-Switching converter can be obtained using the Laplace time delay propriety in (5.7):

$$f(t) \xrightarrow{TL} F(s) \Rightarrow V_p(s) = K_D u_c(s) \;;\; f(t-T_d) \xrightarrow{TL} F(s)e^{-sT_d} \Rightarrow V_p(s) = K_D e^{-sT_d} u_c(s) \tag{5.7}$$

Being:

$$\frac{V_p(s)}{u_c(s)} = K_D e^{-sT_d} \approx \frac{K_D}{e^{sT_d}} \approx \frac{K_D}{1 + sT_d + \frac{s^2 T_d^2}{2!} + \ldots + \frac{s^k T_d^k}{k!}} \approx \frac{K_D}{1 + sT_d} \tag{5.8}$$

5.1 Current controller

Consider that we want to control the inductor's current i_L ($i_L = i_{Lref}$) of a switching converter where the constant current source represents the converters that will be connected:

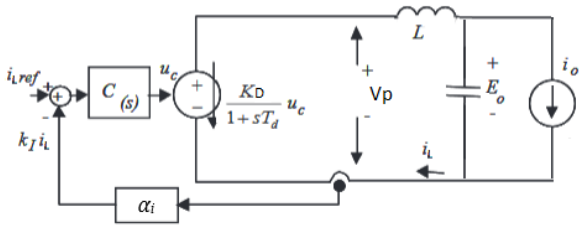

Fig. 5.3 - Equivalent block diagram of the current controlled converter supplying a generic load [14]

The transfer function of the inductor's current can be obtained by applying the Laplace transform to the equations obtained from Kirchhoff's laws:

$$i_L = \frac{V_p - E_0}{sL} \tag{5.9}$$

The block diagram including the current sampling (α_i) and the compensator C(s) is:

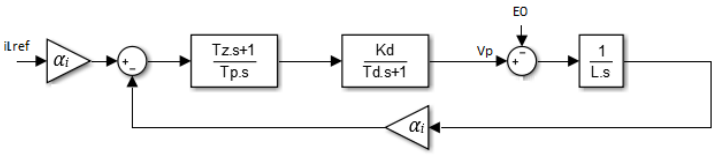

Fig. 5.4 - Block diagram of the linear current controller

A Proportional-Integral compensator was chosen because it ensures a zero-static error when perturbations E_0 occur. The closed-loop transfer function is:

$$i_L(s) = \frac{\left(1+sT_z\right)i_{Lref}(s) - \frac{sT_p(1+sT_d)}{K_D\alpha_i}E_0(s)}{s^3\frac{LT_dT_p}{K_D\alpha_i} + s^2\frac{LT_p}{K_D\alpha_i} + sT_z + 1} \tag{5.10}$$

To ensure stability, the $b_k^2 = a_i b_{k-1} b_{k+1}$ criterion is applied to the denominator [14] to obtain the values of T_p and T_z:

$$\begin{cases} T_z^2 = a_i\dfrac{LT_p}{K_D\alpha_i} \\ \left(\dfrac{LT_p}{K_D\alpha_i}\right)^2 = a_i T_z \dfrac{LT_pT_d}{K_D\alpha_i} \end{cases} \Rightarrow \begin{cases} T_z = a_i^2 T_d \\ T_p = \dfrac{a_i^3 T_d^2 K_D\alpha_i}{L} \end{cases} \tag{5.11}$$

Substituting these results in the polynomial denominator of the closed loop transfer function, it is obtained:

$$\frac{i_L(s)}{i_{Lref}(s)} = \frac{\left(1 + a_i^3 T_d s\right)}{a_i^3 T_d^3 s^3 + a_i^3 T_d^2 s^2 + a_i^2 T_d s + 1} \tag{5.12}$$

The model presented is valid under small disturbances. For large disturbances either the converter saturates or high currents (or voltages) are created. To avoid this situation, a PI compensator with limiter and anti-wind-up reset must be used often.

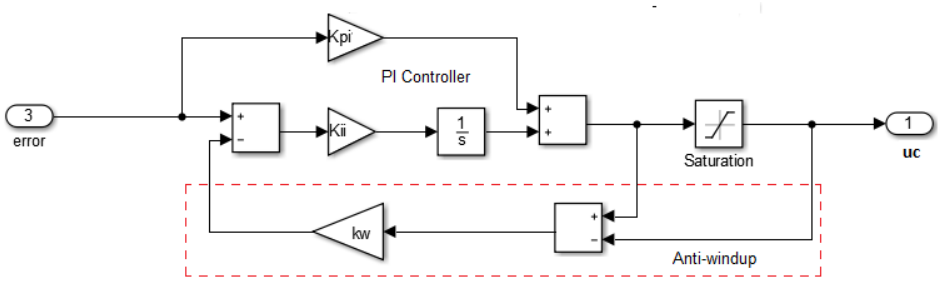

Fig. 5.5 - Current PI compensator with limiter and anti-wind-up reset

The gains K_p and K_i are given by:

$$\begin{cases} K_p = T_z / T_p \\ K_i = 1 / T_p \end{cases} \tag{5.13}$$

The anti-windup gain k_w must be a value chosen between 0 and $\sqrt{K_p K_i}$ [14]. Considering the first order approximation in (5.8), using the root locus diagram it can be seen that the controllers in the current mode are stable for $T_p > K_D k_i T_d/(2R)$, in other words for $\varepsilon > 0.35$. [14]

5.2 Voltage controller with inner current controller

Consider that we want to control again the same switching converter as in Fig. 5.3, but now it is necessary to control the output voltage E_0 as well ($E_0 = E_{0ref}$). To try to present a closed solution, the system order is reduced. It can be written as:

$$\frac{i_L(s)}{i_{Lref}(s)} = \frac{1}{\dfrac{a_i^3 T_d^3 s^3 + a_i^3 T_d^2 s^2 + a_i^2 T_d s + 1}{a_i^2 T_d s + 1}} \tag{5.14}$$

Considering low frequencies, small T_d, and $a_i >> 1$, the transfer function (5.14) may be written as:

$$\frac{i_L(s)}{i_{Lref}(s)} \approx \frac{1}{T_d s\left(\dfrac{a_i^2 - 1}{a_i}\right) + 1} \tag{5.15}$$

This means that the current controller under the above simplifications may be represented as a first order system. Assuming that the voltage is obtained on a capacitor C in parallel with a current source, it is written:

$$E_0(s) = \frac{1}{sC}(i_L(s) - I_0(s)) \tag{5.16}$$

The block diagram of the control system, including the voltage sensor gain (α_v) and a compensator is:

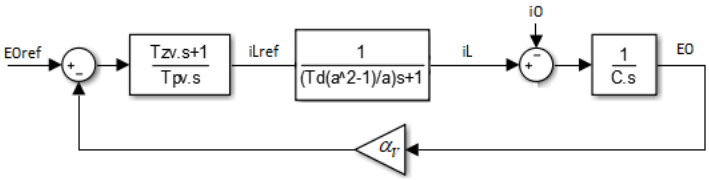

Fig. 5.6 - Block diagram of the output voltage controller

A PI compensator is chosen, as the integral is required to ensure zero static error due to I_0 disturbance and a proportional action is necessary to guarantee a reasonably fast response time.

$$E_0(s) = \frac{(T_{zv}s+1)E_{0ref}(s) - I_0(s)T_{pv}s\left(\left(\frac{a_i^2-1}{a_i}\right)T_d s+1\right)}{\left(\frac{a_i^2-1}{a_i}\right)T_d C T_{pv}s^3 + C T_{pv}s^2 + \alpha_v T_{zv}s + \alpha_v} \tag{5.17}$$

Applying the same criteria to the denominator, $b_k^2 = a_v b_{k-1} b_{k+1}$, the values of T_{pv} and T_{zv} are obtained:

$$\begin{cases} (CT_{pv})^2 = a_v\left(\frac{a_i^2-1}{a_i}\right)T_d C T_{pv}\alpha_v T_{zv} \\ (\alpha_v T_{zv})^2 = a_v C T_{pv}\alpha_v \end{cases} \Leftrightarrow \begin{cases} T_{zv} = a_v^2\left(\frac{a_i^2-1}{a_i}\right)T_d \\ T_{pv} = \dfrac{a_v^3\left(\frac{a_i^2-1}{a_i}\right)^2 T_d^2\alpha_v}{C} \end{cases} \tag{5.18}$$

A PI compensator with limiter and anti-wind-up reset (Fig. 5.7) is chosen, for the reason mentioned in the previous section, where the proportional gain K_{pV} and the integral gain K_{iV} are calculated according to:

$$\begin{cases} K_{pV} = T_{zV} / T_{pV} \\ K_{iV} = 1 / T_{pV} \end{cases} \tag{5.19}$$

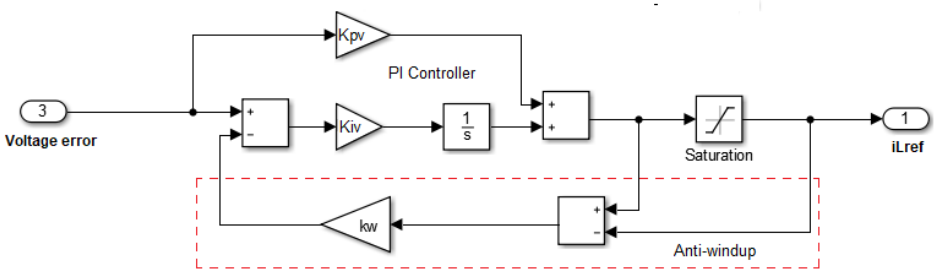

Fig. 5.7 - Voltage PI compensator with limiter and anti-wind-up reset

The developed PI controllers will be used for comparison purposes in the next chapters.

Chapter 6

Obtained Results

In this chapter, simulation results using the three control strategies are presented: Backstepping Sliding Mode Control, Recursive Backstepping Control and Linear Control. Also, experimental results were obtained with BSMC.

6.1 Simulation Results

In this section, both non-linear and linear controllers designed in Chapter 4 and Chapter 5 are discussed and compared. In order to do that, a model of the whole system presented in Chapter 2 was created in MATLAB/Simulink. The value chosen for the DC grid voltage was 380V. Table 6.1 shows the simulation parameters for the main DC/DC converter.

Table 6.1 – Simulation Parameters of the Main Converter

Input Voltage U [V]	Output Voltage V_0 [V]	Rated Power P_0 [W]	L [mH]	r_l [Ω]	C [µF]	r_c [Ω]	f [kHz]	η [%]
540	380	3500	6.3	0.4	5.5	1	20	95

To evaluate if the main DC/DC converter is able to supply the DC grid under a large load variation, three Buck Converters operating at constant power are connected to the DC grid. The following scenario was simulated:

- At *t*=0s Converter 1 is connected to the DC grid
- At *t*=0.05s Converter 2 is connected to the DC grid
- At *t*=0.05s Converter 3 is connected to the DC grid

Converter 1, 2 and 3 have an efficiency of 95% and their switching frequencies are 20kHz, 30kHz and 40kHz, respectively. All the loads have a linear voltage and current controller. It is out of the scope of this thesis to evaluate the performance of the load converter control system thus their controllers will remain the same throughout the simulations. The parameters for each load are displayed in Table 6.2.

Table 6.2 - Simulation Parameters of the Load Converters

DC/DC Converter 1		DC/DC Converter 2		DC/DC Converter 3	
P_{01}	300 W	P_{02}	1300 W	P_{03}	1500 W
V_{01}	300 V	V_{02}	250 V	V_{03}	200 V
C_1	0.17 µF	C_2	0.7 µF	C_3	1.1 µF
L_1	33 mH	L_2	6 mH	L_3	3.3 mH

In the connection to the DC grid, the higher power converters 2 and 3 are equipped with soft-starters to minimize the disturbances in the grid. These soft-starters increase the output reference voltages linearly from 0V to the rated values, taking 0.05s to achieve those values.

As mentioned in Chapter 2 each buck converter has an input filter. The filter topology is represented in Fig. 6.1

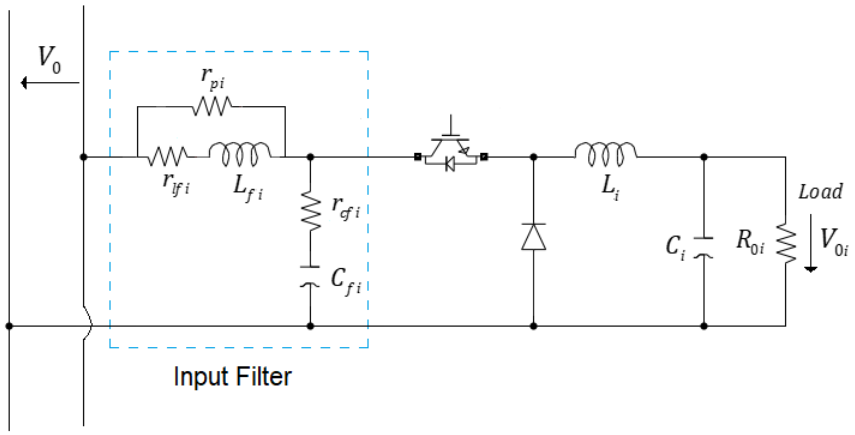

Fig. 6.1 – Topology of the load connected to the DC grid

Table 6.3 shows the values for the inductors and capacitors for each LC input filter of each one of the loads.

Table 6.3 – Values for each one of the loads input LC filter capacitors and inductors

C_{f1} [µF]	L_{f1} [mH]	C_{f2} [µF]	L_{f2} [mH]	C_{f3} [µF]	L_{f3} [mH]
0.65	7	2.3	1.1	2.5	0.7

The parasitic resistances of each one of the loads input filters is presented Table 6.4.

Table 6.4 – Parasitic resistances of the loads input filter

r_c [Ω]	r_l [Ω]	r_{cf1} [Ω]	r_{lf1} [Ω]	r_{cf2} [Ω]	r_{lf2} [Ω]	r_{cf3} [Ω]	r_{lf3} [Ω]
1	0.4	0.022	0.019	0.19	0.006	0.22	0.005

The values obtained for the damping resistor $r_{pi,}$ are displayed in Table 6.5:

Table 6.5 – Damping resistors of the DC loads input filters

r_{p1} [Ω]	r_{p2} [Ω]	r_{p3} [Ω]
65	12	10

In Appendix A all the formulas used to calculate the components and parameters necessary to run the simulations are presented.

6.1.1 Linear Controllers

In this section, the simulation results using linear controllers (Chapter 5) are exhibited. The values for a_i and a_V from equations (5.11) and (5.18) are 10 and 2 respectively, and the compensator gains are displayed in Table 6.6.

Table 6.6 – PI current and voltage controller parameters

Current controller		Voltage Controller	
K_i	18.67	K_{iV}	11.45
K_p	0.0467	K_{pV}	0.0113
k_{wi}	0.9	k_{wV}	0.3

Fig. 6.2 shows the DC grid voltage and current. It is possible to see that after the connection of converter 1, the voltage at the DC-Link reaches the desired output voltage, 380V at approximately 0.03s. However, when converters 2 and 3 are connected, linear controllers are unable to guarantee the stability of the grid.

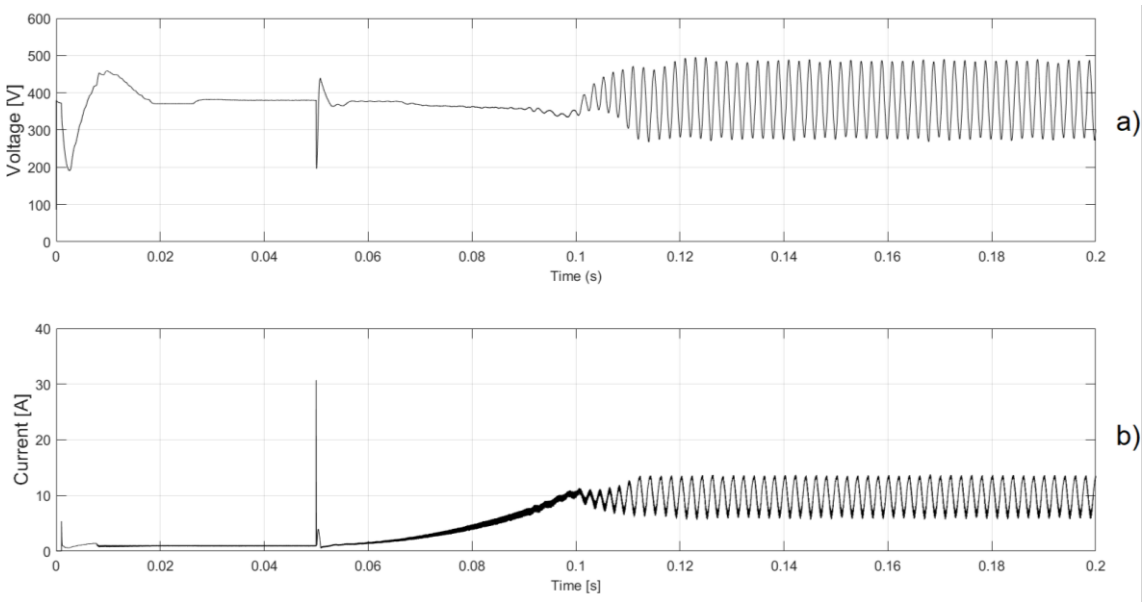

Fig. 6.2 – Voltage and current waveform in the DC grid using Linear Controllers a) DC grid voltage; b) DC grid current

The current spikes seen at *t*=0s and *t*=0.05s result from the fact that when the load converters are connected to the grid, their input filters are not charged. Considering an abrupt load variation and using linear controllers, the solution to guarantee constant voltage in the DC grid would be to resize the main DC/DC converter output filter capacitor C [14]. This would result in a much higher capacitor value ($C \approx$ 350μF) than the one presented in Table 6.1. However, the results have improved and the system does not present an oscillatory response (Fig. 6.3). The formula used to calculate the value of this new capacitor can be found in Appendix A.

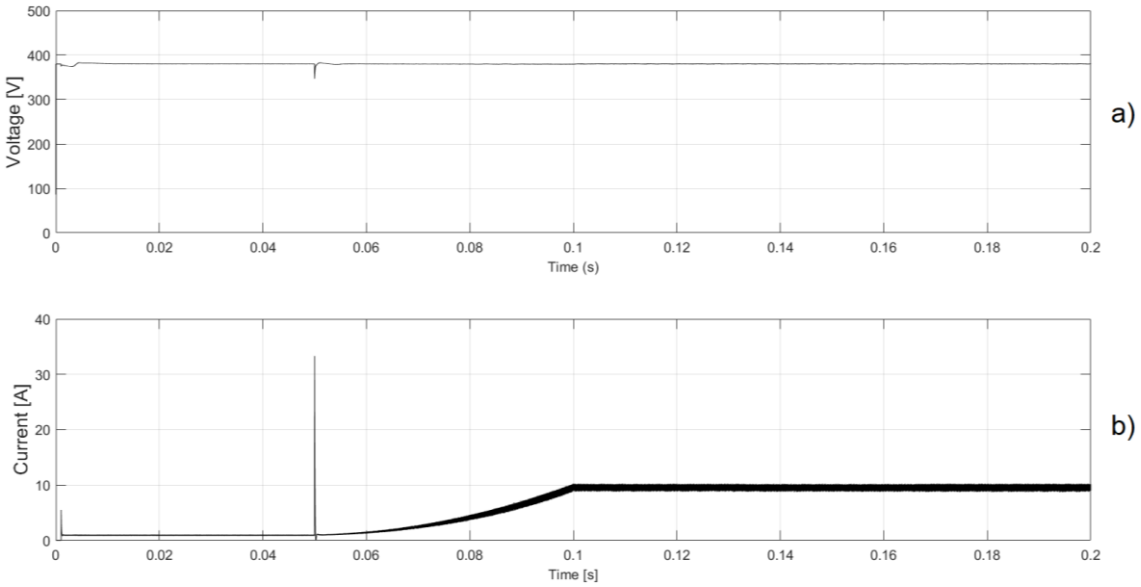

Fig. 6.3 - Voltage and current waveform in the DC grid using Linear Controllers and C≈350μF:
a) DC grid voltage; b) DC grid current

6.1.2 Backstepping Sliding Mode Control

The results from using the BSMC design discussed in section 4.1 are presented here. According to Lyapunov's second method, the only requirement to choose the value for k_v from equation (4.10) is $k_v > 0$. By looking at expression (4.8), it can be seen that the solution to that differential equation is given by:

$$e_{v_c} = ce^{-k_v t} \tag{6.1}$$

Where *c* is a constant. This means that the higher the value k_v, the lower the time constant is, resulting in a system that achieves its steady state much faster. However, in terms of control systems, the outer loop (i.e. Voltage controller) must be slower than the inner loop (i.e. Current controller) in order to decouple both dynamics [23] [24]. In steady state, for the chosen operating point, the switching frequency was close to 20kHz. Therefore, the time constant τ must be higher than 0.05ms (1/20kHz). The value chosen for k_v was 10000, which corresponds to τ=0.1ms.

From Fig. 6.4, it can be seen that the output voltage reaches its expected value (380V) after the connection of the high-power converters at *t*= 0.05s. Also, it can be seen that this non-linear

method, greatly reduces the settling time comparing to Fig. 6.3 and that the output voltage ripple becomes lower and has an amplitude of 2V.

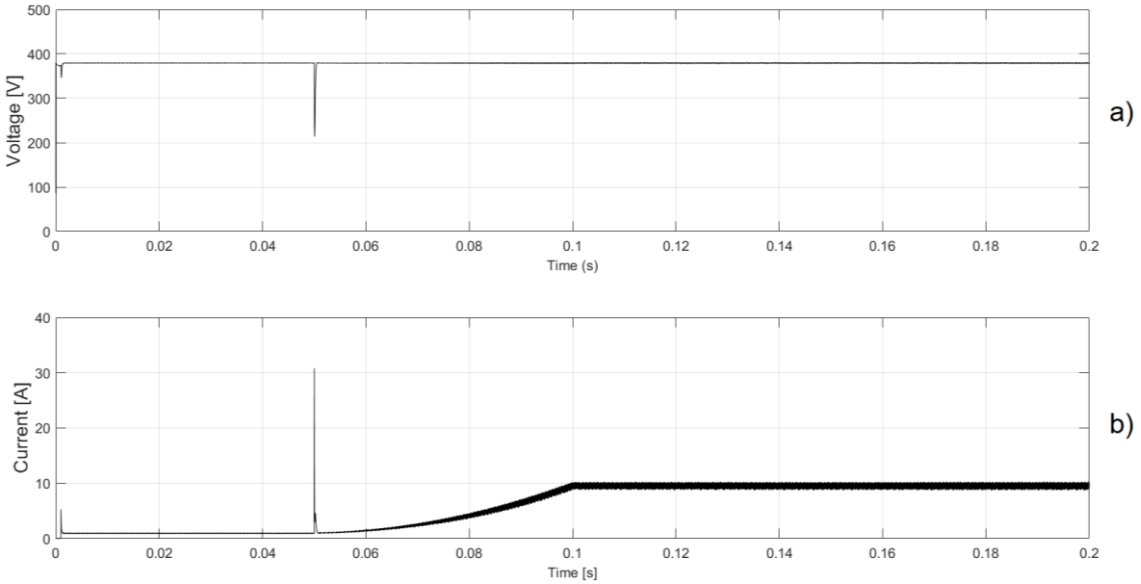

Fig. 6.4 Voltage and current waveform in the DC grid using the BSMC
a) DC grid voltage; b) DC grid current

It is worth noting that the value of the main capacitor is the same presented in Table 6.1 (C =5.5 μF), it is not necessary to increase its value by 60 times to produce acceptable results. The voltage dip is mainly caused due to the fact that the input filters of the loads are not charged when the load is connected to the grid.

Fig. 6.5 represents the output voltage of every load converter mentioned in Table 6.2. It can also be seen the soft starter working in converter 2 and 3.

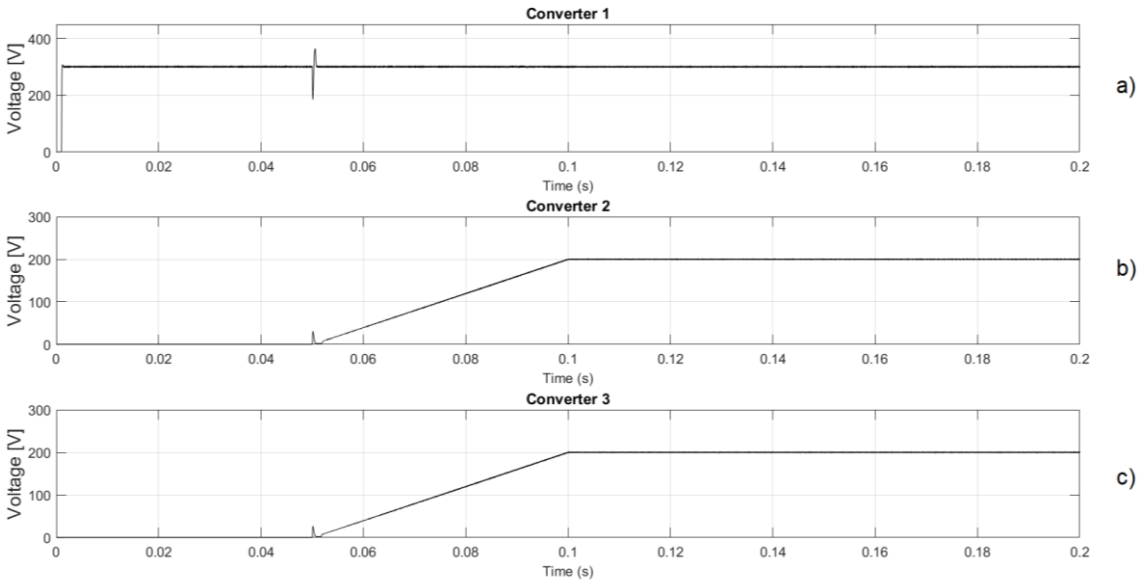

Fig. 6.5 –Load output voltage waveforms a) Converter 1 voltage; b) Converter 2 voltage; c) Converter 3 voltage

The system presents no steady state error. However, errors can be observed if there is an offset or another error in one of the measurements. The next picture shows the same experiment but with an error in the output current measurement (I_0) of 20%. The DC grid voltage is shown and it can be seen that there is a steady state error of 40V and the system is unable to reach the desired output voltage.

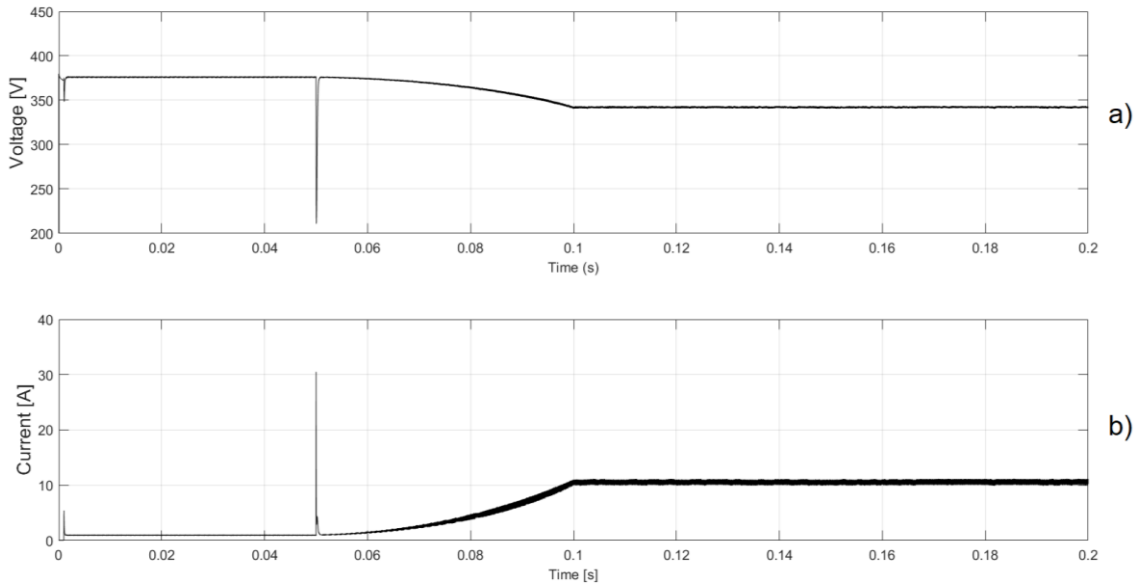

Fig. 6.6 - Voltage and current waveforms in the DC grid using the BSMC with a measurement error
a) DC grid voltage; b) DC grid current

One way to solve this problem is to include an integral action in the controller. The result of using the voltage controller presented in section 4.1.1.2 is shown in Fig. 6.7.

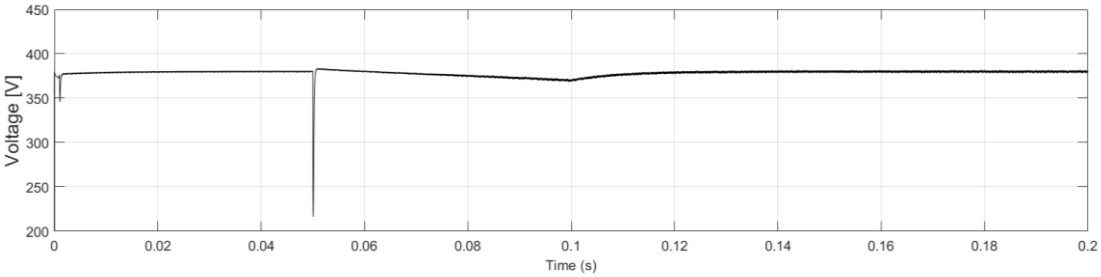

Fig. 6.7 - Voltage waveform in the DC Grid using the BSMC with a measurement error

It is visible that the integral part of the control system contributed to nearly eliminate the steady state error thus bringing the system to the desired equilibrium point. It should be kept in mind that the soft-starter is working from *t*=0.05s to *t*=0.1s and that is why there is a clear change in the voltage's slope at *t*=0.1s.

6.1.3 Recursive Backstepping Control

Fig. 6.8 represents the same test performed in section 6.1.1 and 6.1.2 but using controllers based on backstepping control theory. In order to compare both methods under the same conditions, the gain chosen for k_v, from equation (4.26) and (4.36), was also 10000. It is common practice to select the inner loop gains higher than the output loop gains to achieve good tracking performance [23] [24] (i.e. $k_i > k_v$), thus the value chosen for k_i was 100000.

It can be seen in Fig. 6.8, that very good results can be obtained with this controller. However, if we observe the switching frequency in Fig. 6.9, it is visible that there is more than one commutation in one PWM period. This unrealistic switching frequency leads to higher losses and therefore worst efficiencies.

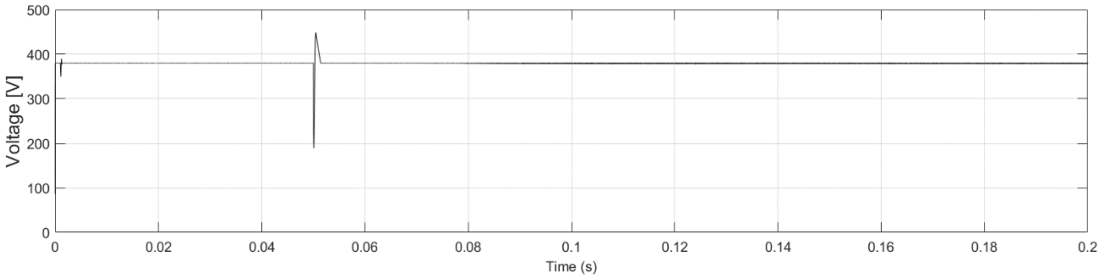

Fig. 6.8 - Voltage and current waveform in the DC grid using the RBC

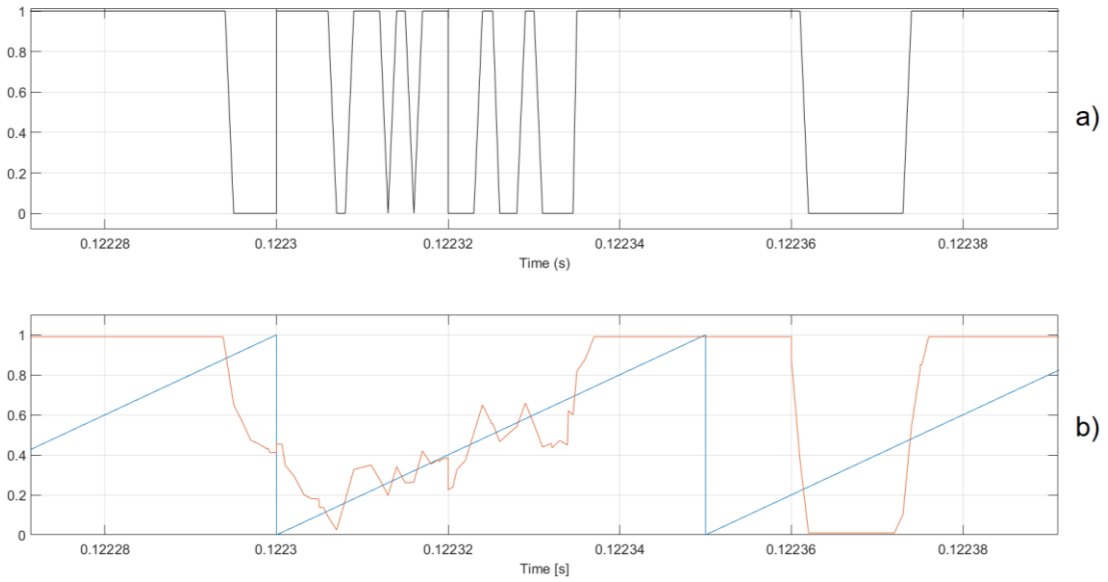

Fig. 6.9 – a) Switching frequency of the main DC Converter;
b) Sawtooth Modulator: Carrier (Red) and Modulating Signal (Blue)

In order to solve this problem, a constant frequency modulator was designed. This modulator guarantees that in a PWM cycle, the converter does not switch more than once. Using this new modulator, the voltage and current in the DC link are displayed in the following figure:

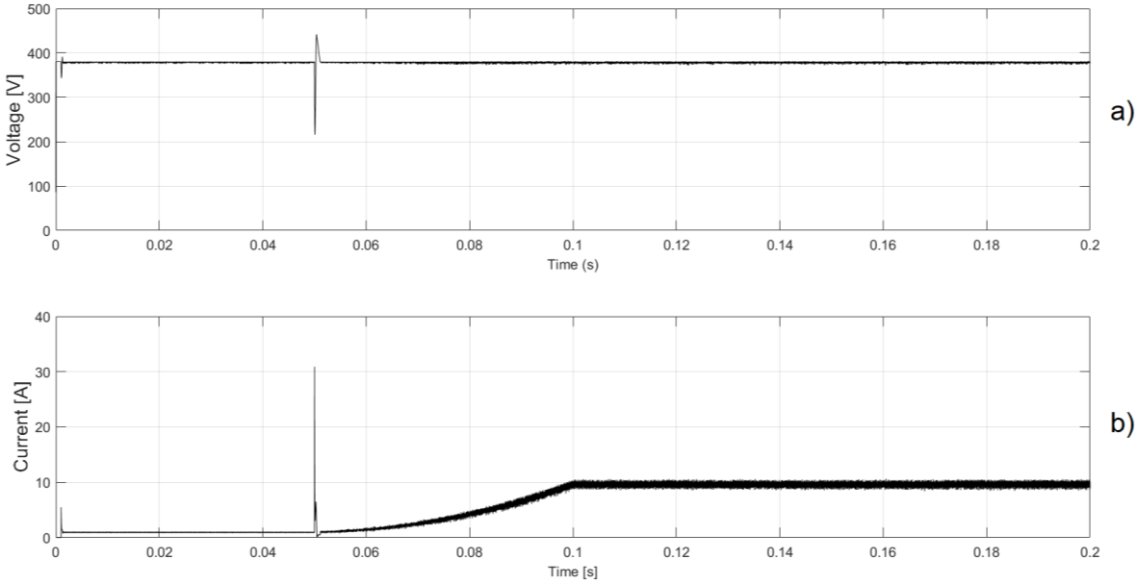

Fig. 6.10 - Voltage and current waveform in the DC Grid using the RBC
with a constant frequency modulator: a) DC grid voltage; b) DC grid current

Fig. 6.10 demonstrates that the DC grid voltage reaches its equilibrium point (380V) quite fast after a disturbance in the grid. After the connection of converter 2 and 3, the system has 20% overshoot but the control system is able to return to the steady state with a settling time of 1ms. The output voltage waveform of every load converter is equal to Fig. 6.5, so for the conciseness it is not displayed.

The results of having an error of 20% in the measurement of the output current are expressed in Fig. 6.11. It is clear that this controller eliminates the steady-state error as opposed to the controller BSMC described in the previous section.

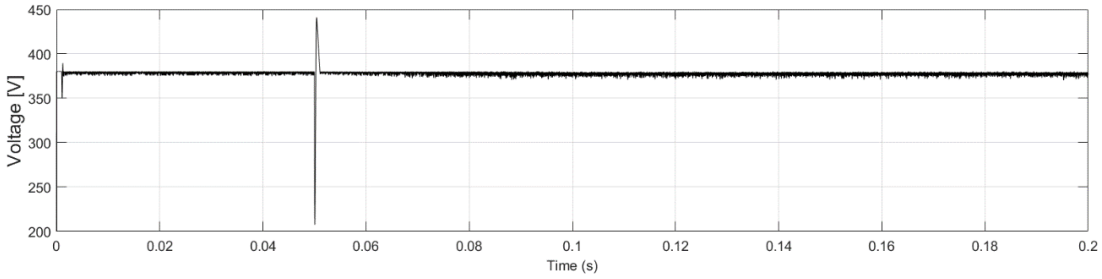

Fig. 6.11 - Voltage waveform in the DC Grid using the RBC with a measurement error

6.1.4 Short Circuit in the grid and in the loads

A circuit breaker is equipped in every load converter and should be able to, in a case on a short-circuit in the respective load, open the circuit as fast as possible, in order to not disturb too much the DC grid current and voltage.

In this thesis, the circuit breaker (CB) has been modelled as an ideal switch that will open the circuit if the input current of one of the loads has surpassed its correspondent maximum threshold, during a short time interval. This way it is guaranteed that, when a large current spike occurs due to a load connection to the grid, the CB will not operate to open the circuit since the input current only exceeds its threshold during a short amount of time.

The next figure shows the voltage and current in the DC-grid when a pole-to-ground fault is applied to the second load converter 2 at t=0.1s.

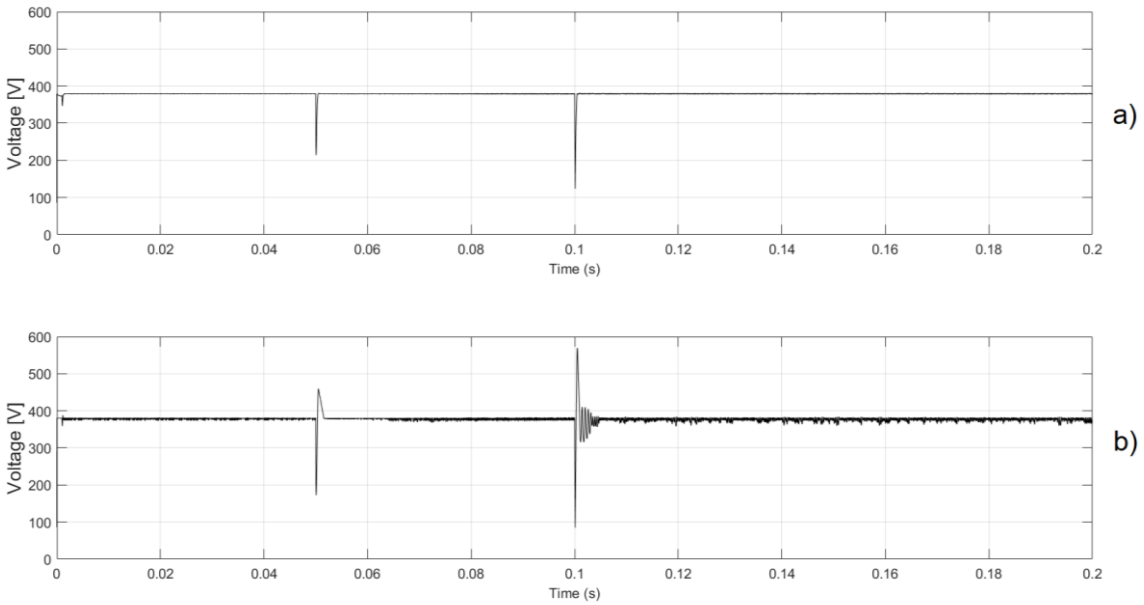

Fig. 6.12 – Pole-to-ground fault in the converter 2 a) using the BSMC; b) using the RBC

After a short circuit at the input of DC-DC converter 2 a high current spike is detected, the corresponding CB clears the fault by disconnecting the respective load. As seen in both figures above, the main control system is still able to maintain the desired voltage after an abrupt load variation. However, the results also show that the second load induces a large overshoot (≈50%).

The main circuit breaker is supposed to interrupt the current flow when a fault or short circuit occurs in the DC grid, and if the maximum threshold, which is 1.5 times higher than the main converter's nominal current, is exceeded during 0.1ms (approximately two switching periods). A robust control system should restore the voltage back to its nominal value after the fault on the DC-bus disappears. To restore the DC grid back a recloser is used. A recloser is a special type of CB that has the ability to restore the power automatically in temporary fault situations. A recloser has been simulated in which the number of reclose attempts is limited to a maximum of three in equally spaced time intervals of 0.05s.

Fig. 6.13 shows a short-circuit on a charged power line at t=0.1s and lasts 0.06s. It can be seen that at t=0.15s the main CB tries to reclose but fails since the short circuit is not extinguished. However, at t=0.2s, the short-circuit has disappeared and all the converters are supplied.

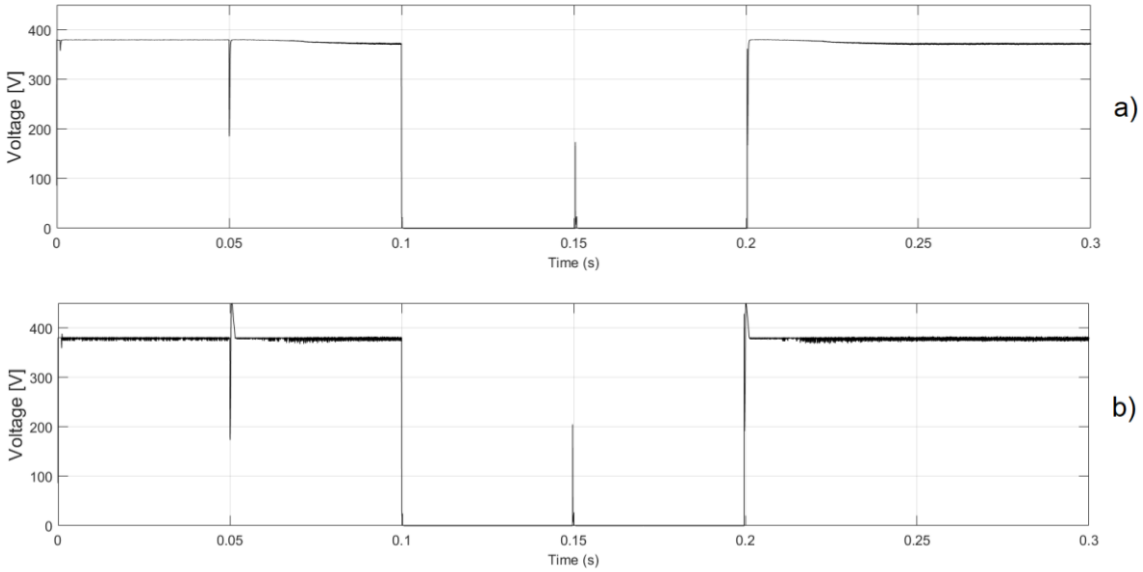

Fig. 6.13 – Pole-to-ground fault in the Grid a) using the BSMC; b.) using the RBC

6.1.5 Load LC input Filter

In this section, the effect that the input LC filters of each load have on the DC grid voltage is shown. The next picture illustrates the same test as before, but now without using any input filter.

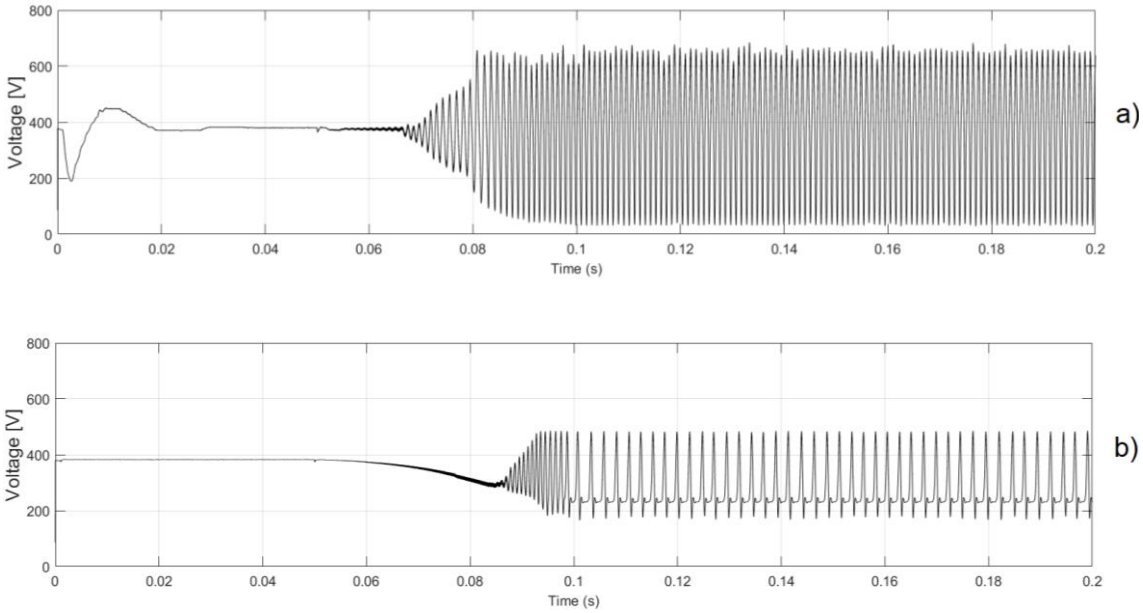

Fig. 6.14 Voltage waveform in the DC Grid without using the input filter in the loads. a) using Linear Controllers. b) using BSMC

Fig. 6.14 shows why is it important to use an input filter on each load. It is clear that after the connection of Load converter 2 and 3 the results are not acceptable and the DC line is not

regulated. In Fig. 6.15 an LC ideal filter (without any damping resistors) was added at the input of the loads and the results are the following:

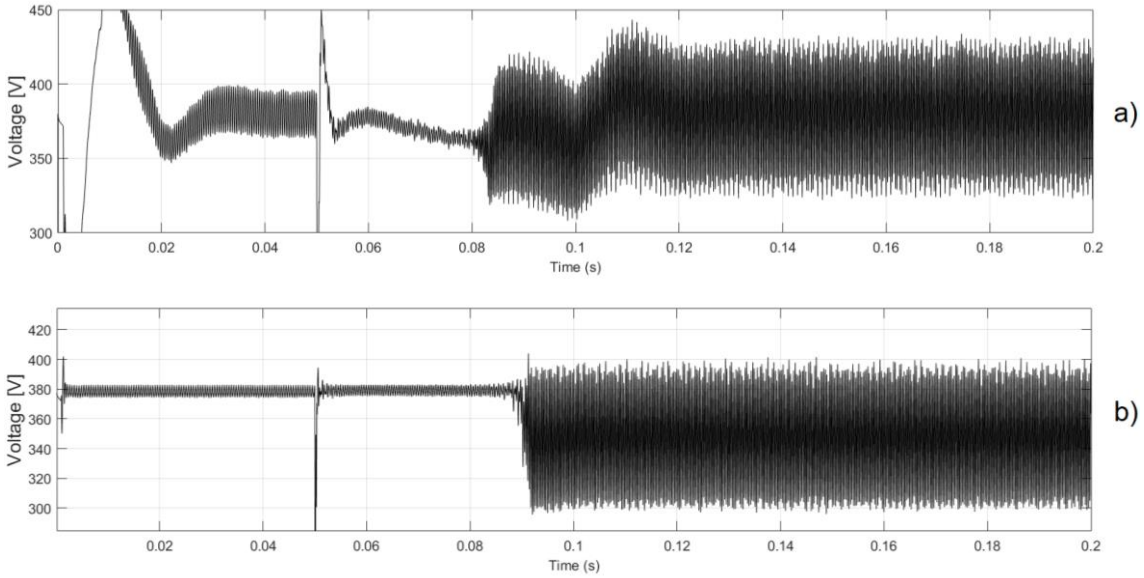

Fig. 6.15 a) using Linear Controllers. b) using the BSMC

Comparing Fig. 6.15 and Fig. 6.14 it is evident that the ideal input filter improves the results. Still, they do not have damping and therefore are not acceptable since the output voltage ripple has an amplitude of 100V using both linear controllers and BSMC.

This effect could be minimized by using a higher capacitor value in the main converter. However, having high value capacitors in the DC grid is not one of the objectives of this thesis. To reduce these oscillations, damped filters as the one presented in Fig. 6.1 were connected at the input of each one of the DC-DC loads. The results were already presented in Fig. 6.2 and Fig. 6.4, but Fig. 6.16 illustrates a more detailed part of those figures for a better visualization.

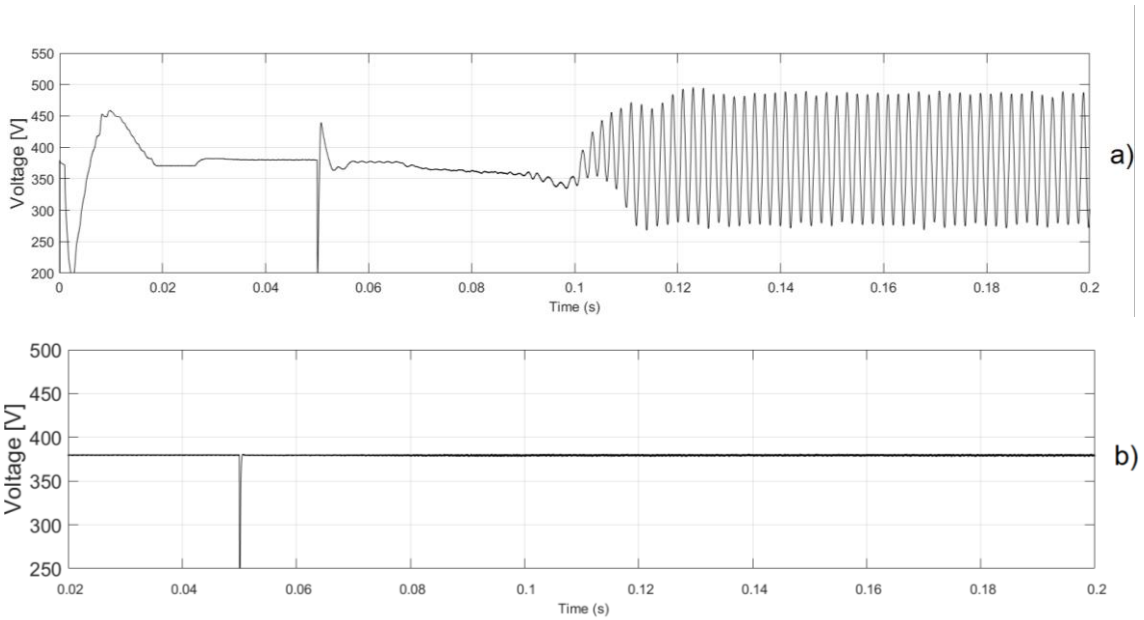

Fig. 6.16 - Voltage waveform in the DC Grid: a) using Linear Controllers. b) using the BSMC

It is visible the effect of adding a well-sized input filter to the system using BSMC (Fig. 6.16 b)). This will change the dynamics of the converter resulting in a more stable system. However Linear Controllers are unable to regulate the DC grid even with an appropriately damped input filter.

6.2 Experimental Results

On a much smaller scale, due to lab and time restritions and available materials, the results obtained with the Backstepping Sliding Mode Controller on Simulink were reproduced in the Electrical Energy laboratory of Instituto Superior Técnico. As seen in this chapter, using the RBC with a constant frequency modulator may lead to overvoltages and a higher voltage ripple. This, combined with other practical issues such as slow hardware, prevented experimental results using the recursive backstepping controller from being obtained.

The DC-link voltage was chosen to be 19V, and the control scheme was implemented in a Microchip dsPIC33EP512MU810. The microprocessor receives as input the measurements of the inductor current, DC grid and DC grid voltage, and has the task of producing the driving signal for the transistor located in the main DC-DC Converter.

The constant power load used in this experiment was an HP laptop without using its battery and with a power consumption of 23W. Additionally a 50 ohms (7W) resistive load was connected to the DC grid.

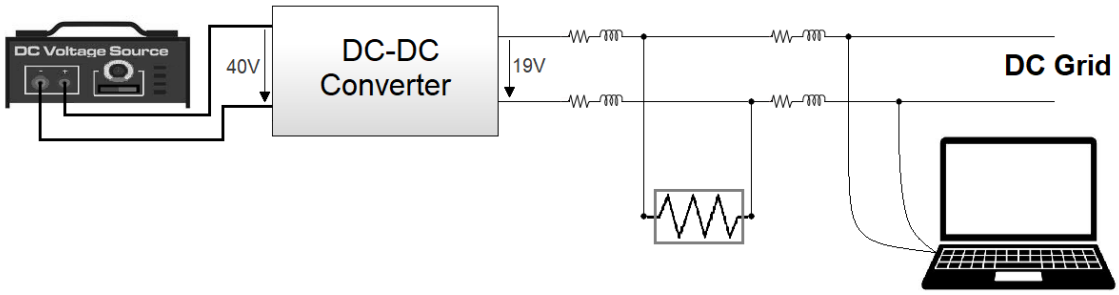

Fig. 6.17 – Laboratory DC grid representation

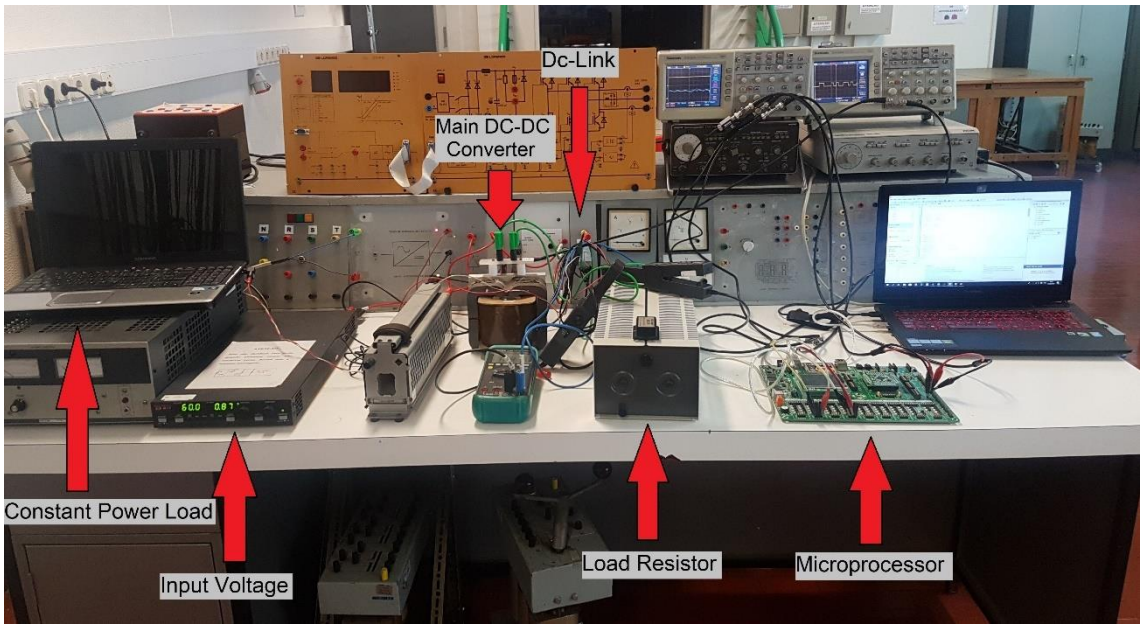

Fig. 6.18 – Laboratory Set-up

Table 6.7 - Laboratory Parameters of the Main Converter

Input Voltage U [V]	Output Voltage V_0 [V]	L [mH]	C [µF]
40	19	15	1000

Fig. 6.19 depicts the voltage in the DC grid with a resistor as a load (Fig. 6.19 a)) and with a resistor and one laptop as a load (Fig. 6.19 b)). It is clear that after turning on the laptop to the grid the current increases but the DC voltage remains the same.

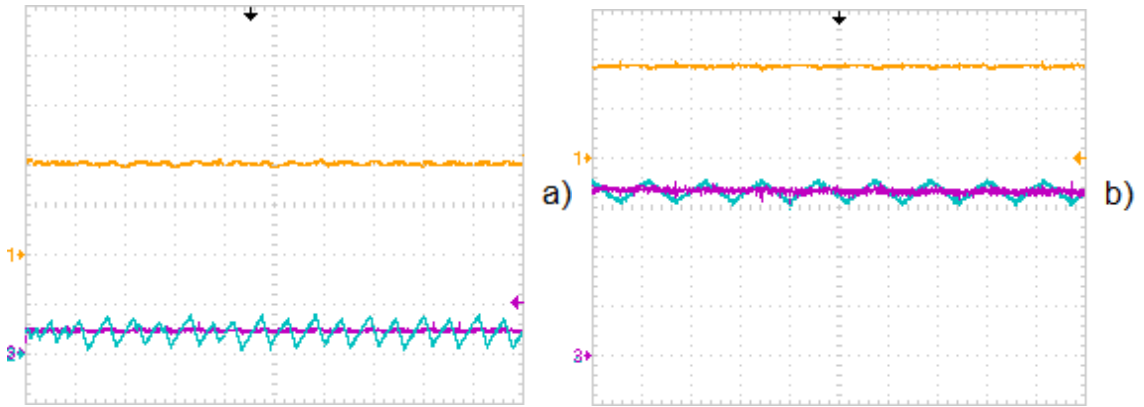

Fig. 6.19 - DC grid voltage and current waveforms, and inductor's current in the main DC/DC converter: a) Using a resistive load; CH1 (orange): DC grid voltage waveform (10V/div); CH2 (blue): Inductor's current waveform (1A/div); CH3 (purple): DC grid's current waveform (1A/div). *t* (2.5 ms/div) b) Using a resistive load and a laptop computer; CH1 (orange): DC grid voltage waveform (10V/div); CH2 (blue): Inductor's current waveform (0.5A/div); CH3 (purple): DC grid's current waveform (0.5A/div). *t* (250 µs/div)

In Fig. 6.20 the input voltage U in the main converter (Fig. 2.1) is increased from 40V to 60V resulting in a smaller duty cycle. Despite the input voltage increase, Fig. 6.20 shows that the voltage in the DC grid remains nearly constant at around 19V with the laptop turned on and connected to the grid, and the resistive load connected to the grid as well.

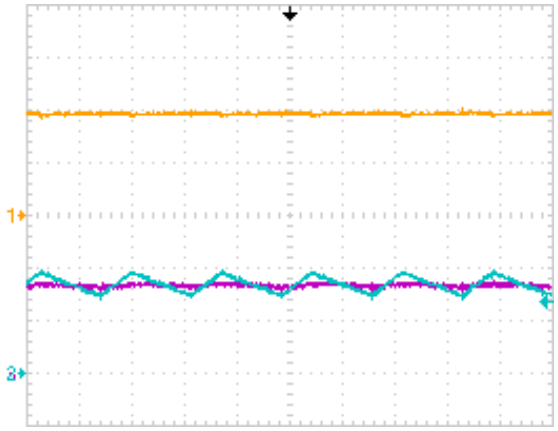

Fig. 6.20 - Results obtained for the DC grid voltage and current, and inductor's current in the main DC/DC converter; CH1 (orange): DC grid voltage waveform (10V/div); CH2 (blue): Inductor's current waveform (1A/div); CH3 (purple): Grid's current waveform (1A/div) *t* (250 µs/div)

Fig. 6.21 represents the transient response of the voltage and current in the DC grid. Fig. 6.21.a) shows the transient when the laptop is turned on, and Fig. 6.21 b) shows the transient when the laptop is turned off.

The DC grid voltage waveform is zoomed on purpose to show that after the connection/disconnection of the laptop the controller is still able to track the desired value.

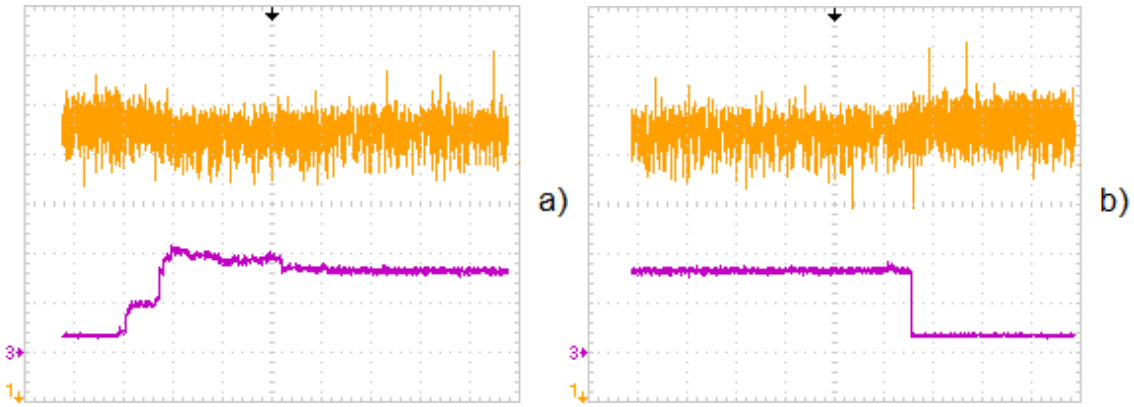

Fig. 6.21 - Transient response of DC grid voltage and current: a) Transient when the laptop is turned on; b) Transient when the laptop is turned off. CH1 (orange): DC grid voltage (500mV/div), CH3 (purple): DC grid current (1A/div) *t* (1s/div)

The next figure presents the transient response of the grid voltage when two laptops are connected to the DC-link. The second load connected is another HP laptop with a power consumption of 23W.

Fig. 6.22 - Transient response of DC grid voltage and current when the two laptops are turned on; CH1 (Orange): DC grid voltage (5V/div) CH2 (Blue): Inductor's current waveform (0.5A/div) *t* (50ms/div)

There is no voltage sag in the figures above mainly because the value of the capacitator is around 20 times higher than necessary.

Chapter 7

Conclusions

In this chapter, the conclusions of the developed work and the perspectives of future work are presented.

7.1 Final Conclusions

The objective of this Master Thesis was to design non-linear controllers for a DC-DC converter that supplies power to a DC microgrid in order to reduce the capacitance of the DC line stabilizing capacitor. Ensuring the stability of the DC distribution system can be a challenging problem due to the connection of Constant Power Loads that tend to destabilize his feeder. Two different non-linear control systems were designed in order to counteract the nonlinearities induced by CPL. The controller's performance is evaluated based on the stability of the DC grid voltage and their transient and dynamic response when a disturbance occurs.

Results were also obtained using the well-known and popular Linear Controllers. These controllers present an overshoot and reasonably high settling times but, under small load variations, they are able to track the desired values. However, when a large load variation occurs, linear controllers often lose the ability to reach a stable steady state without using a very large DC line capacitor. To overcome this, two nonlinear controllers were designed and implemented.

The first non-linear controller proposed is based on Lyapunov's control theory. Backstepping combined with Sliding Mode (BSMC) have shown a good tracking performance and settling time was found to decrease significantly compared to linear controllers. On the other hand, the results also evidence a steady state error if an error in the measurement of one of the state variables is present. This controller can be modified to eliminate this steady state error by adding an integral action.

The second non-linear controller also uses Lyapunov's theory to build a recursive backstepping controller. This new controller showed robustness towards parameter variations, disturbances and measurement noise. In all the tests performed there was no steady state error but at the same time, all the tests performed presented an overshoot and a higher voltage ripple when compared to BSMC.

Both the Backstepping Sliding Mode Controller and Recursive Backstepping Controller guaranteed the stability of the DC distribution grid. Through comparative computer simulations,

the best performance was obtained with BSMC. Experimental studies conducted on the laboratory of Instituto Superior Técnico validate the proposed BSMC controller.

The main recommendation of this thesis is, therefore, to use non-linear controllers, based on backstepping and/or sliding mode, to deal with the constant power loads of DC grids, and to allow a significant reduction in the DC line capacitance.

7.2 Future Work

For future research, it would be interesting to study and investigate a closer model to real operating conditions with more CPLs connected and with renewable sources injecting power to the DC grid and a reversible converter.

Related to work laboratory, the step forward would be to increase the voltage in the DC link to higher values. To do that the DC-DC converter used in the laboratory which was not intended for this application, should be properly sized in order to meet the grid and load specifications

In this dissertation only one controller was tested in the laboratory. Experimental results obtained with BSMC motivate to more experimental tests in order to find its limits. To further improve the performance, it can be worth considering adding an integral action. It would be interesting to see experimental results with the other non-linear control system (Recursive Backstepping Controller) and with Linear Controllers and compare the experimental among them.

Bibliography

[1] P. Fairley, “IEEE Sptectrum,” 15 Nov. 2012. [Online]. Available: https://spectrum.ieee.org/tech-history/dawn-of-electronics/san-franciscos-secret-dc-grid.

[2] D. J. Becker and B. J. Sonnenberg, “400 Vdc Power Distribution: Overcoming the Challanges,” in *IEEE 32nd International Telecommunocations Energy Conference*, Orlando, Florida, USA, 2010.

[3] G. Iwanski, P. Staniak and W. Koczara, “Power management in a DC microgrid supported by energy storage,” in *2011 IEEE International Symposium on Industrial Electronics*, Gdansk, Poland, 2011.

[4] B. Glasgo, I. L. Azevedo and C. Hendrickson, “How much electricity can we save by using direct current circuits in homes? Understanding the potential for electricity savings and assessing feasibility of a transition towards DC powered buildings,” *Applied Energy,* vol. 180, pp. 66-75, 15 Oct. 2016.

[5] M. Al-Nussairi, R. Bayindir, P. Sanjeevikumar and P. Siano, “Constant Power Loads (CPL) With Microgrids: Problem Definition, Stability Analysis and Compensation Techniques,” *Energies,* vol. 10, no. 10, Oct. 2017.

[6] G. Paraiso, J. F. Silva and S. F. Pinto, “Control strategies for low voltage DC residencial grids with constant power loads,” in *2018 International Young Engineers Forum (YEF-ECE)*, Lisbon, Portugal, May 2018.

[7] L. Herrera, W. Zhang and J. Wang, “Stability Analysis and Controller Design of DC Microgrids With Constant Power Loads,” *IEEE Transactions on Smart Grid,* vol. 8, no. 2, pp. 881-888, 2017.

[8] J. Liu, W. Zhang and G. Rizzoni, “Robust Stability Analysis of DC Microgrids With Constant Power Loads,” *IEEE Transactions on Power Systems,* vol. 33, no. 1, pp. 851-860, Jan. 2918.

[9] “Future Residential LVDC Power Distribution Architectures,” Aalborg University, [Online]. Available: https://www.et.aau.dk/research-programmes/microgrids/activities/future-residential-lvdc-power-distribution-architectures/.

[10] D. Shuai, Y. Xie and X. Wang, “Optimal control of Buck converter by state feedback linearization,” in *2008 7th World Congress on Intelligent Control and Automation*, Chongqing, China, Aug. 2008.

[11] L. Setyawan, W. Peng and X. Jianfang, “Implementation of sliding mode control in DC microgrids,” in *2014 9th IEEE Conference on Industrial Electronics and Applications*, Hangzhou, China, June 2014.

[12] J. F. Silva, “"Input filter design for power converters" Texto Complementar da disciplina SAA,” 2012. [Online]. Available: https://fenix.tecnico.ulisboa.pt/downloadFile/3779578920509/input%20LC%20filters__.pdf.

[13] M. U. Iftikhar, D. Sadarnac and C. Karimi, “Input Filter Damping Design for Control Loop Stability of DC-DC Converters,” in *2007 IEEE International Symposium on Industrial Electronics*, Vigo, Spain, 2007.

[14] J. F. Silva, “Electrónica Industrial Semicondutores e Conversores de Potência, série Manuais Universitários,” Lisboa, Fundação Calouste Gulbenkian, 2013, pp. ISBN 978-972-31-1499-7, 740.

[15] H. Pang and M. Pong, “A Life Prediction Scheme for Electrolytic Capacitors in Power Converters Without Current Sensor,” in *25th Anual IEEE Aplied Power Electronics Conference and Exposition (APEC) pp.973-979*, Palm Springs, USA, Feb. 2010.

[16] H. K. Khalil, Nonlinear Systems, New Jersey, USA: Prentice Hall.

[17] V. Utkin, “Sliding Mode Design Principles and Applications to Electric Drives,” *IEEE Transactions on Industrial Electronics,* vol. 40, no. 1, pp. 23-26, Jan. 1993.

[18] J. F. Silva and S. F. Pinto, “Control Methods for Switching Power Converters,” in *Power Electronis Handboonk*, 2nd Edition ed., Editor M. H. Rashid, Academic Press, ELSEVIER, USA, ISBN 13:978-0-12-088479-7, ISBN 10:0-12-088479-8, 2007, pp. Chapter 34 , pp 935-998.

[19] P. V. Kokotovic, “The joy of feedback: nonlinear and adaptive,” *IEEE, Control Systems Magazine,* vol. 12, no. 33, pp. 7-17, 1992.

[20] S. Zhang and W. Qian, “Dynamic backstepping control for pure-feedback nonlinear systems,” *CoRR abs/1706.08641,* 2017.

[21] A. D. Martin, J.M.Cano, F. A. Silva and J. R. Vazquez, “Backstepping Control of Smart-grid Connected Distributed Photovoltaic Power Suplies for Telecom Equipment,” *IEEE Transactions on Energy Conversion,* no. 99, 2015.

[22] S. Kozák, “From PID to MPC: Control engineering methods development and applications,” in *2016 Cybernetics & Informatica (K&I)*, Levoca, Slovakia, 2016.

[23] E. V. Oort, L. Sonneveldt, Q. Chu and J. Mulder, “Full Envelope Modular Adaptive Control of a Fighter,” in *AIAA Guidance, Navigation, and Control Conference*, Toronto, Canada, Aug. 2010.

[24] G. F. Trigo, “Robust and Adaptive Nonlinear Attitude Control of a Spacecraft,” Instituto Superior Técnico, Universidade de Lisboa, Mcs Thesis, Lisboa, Portugal, Oct. 2011.

[25] K. Garbesi, V. Vossos and H. Shen, “Catalog of DC Appliances and Power Systems,” Berkeley, California, USA, Oct. 2001.

Appendix A

MATLAB/Simulink variables:

Table A.1 – Filter and controller values used in the simulation of the DC grid

Name	Value	Name	Value
α_i	1	L_{f1} [mH]	7.1
α_V	1	L_{f2} [mH]	1.1
C [µF]	5.61	L_{f3} [mH]	0.72
C_1 [µF]	0.17	P_0 [W]	3500
C_2 [µF]	0.78	P_{01} [W]	300
C_3 [µF]	1.10	P_{02} [W]	1300
C_{f1} [µF]	0.66	P_{03} [W]	1500
C_{f2} [µF]	2.28	R_{01} [Ω]	300
C_{f3} [µF]	2.47	R_{02} [Ω]	48.08
f [kHz]	20	R_{03} [Ω]	26.67
f_1 [kHz]	20	r_C [Ω]	1
f_2 [kHz]	30	r_{Cf1} [Ω]	0.022
f_3 [kHz]	40	r_{Cf2} [Ω]	0.19
K_i	18.67	r_{Cf3} [Ω]	0.22
K_{iV}	11.45	r_l [Ω]	0.4
K_p	0.0467	r_{lf1} [Ω]	0.019
K_{pV}	0.0113	r_{lf2} [Ω]	0.006
k_{wi}	0.9	r_{lf3} [Ω]	0.005
k_{wV}	0.3	U [V]	540
L [mH]	6.3	V_0 [V]	380
L_1 [mH]	32.2	V_{01} [V]	300
L_2 [mH]	5.8	V_{02} [V]	250
L_3 [mH]	3.3	V_{03} [V]	200

To size the inductors and capacitors for the DC-DC converters the following equations were used [14]:

$$L = \frac{U - V_0}{\Delta i_L} \delta T \tag{A.1}$$

$$C = \frac{U\delta(1-\delta)T^2}{8L\Delta V_0} \tag{A.2}$$

The formulas used to calculate the input filter capacitors and inductors for each load were [12]:

$$L_{fi} = \frac{T_i^2 I_{0i}}{32 C_{fi} \Delta i_{Li}} \tag{A.3}$$

$$Cf_i = \frac{2T_i^2 I_{0i}}{4\Delta V_{0i}} \tag{A.4}$$

Considering an abrupt load variation, the formula to calculate the value of the main capacitor is [14]:

$$C = \frac{LP_0^2}{2V_0^2(U - V_0)\Delta V_0} \tag{A.5}$$

To calculate r_{pi} the following equation with a damping ratio of 0.8 was used:

$$r_{pi} = \frac{1}{2\xi}\sqrt{\frac{L_{fi}}{C_{fi}}} \tag{A.6}$$

The formula used to determine the converter's nominal current is:

$$I_{0i} = \frac{P_{0i}}{V_{0i}} \tag{A.7}$$

The length of the line that connects the main converter to converter 1 is 10m, the length of the line that connects converter 1 to converter 2 is 5m, length of the line that connects converter 2 to converter 3 is 2m. The values used for resistance per unit length and inductance per unit length were 0.1Ω/m and 1µH/m respectively.

Table A.2 – Lengths and values of the DC line impedances feeding the loads

Name	Value	Name	Value	Name	Value
d_{M-1}	10 m	r_{line1}	1 Ω	L_{line1}	10 µH
d_{1-2}	5 m	r_{line2}	0.5 Ω	L_{line2}	5 µH
d_{2-3}	2 m	r_{line3}	0.2 Ω	L_{line3}	2 µH

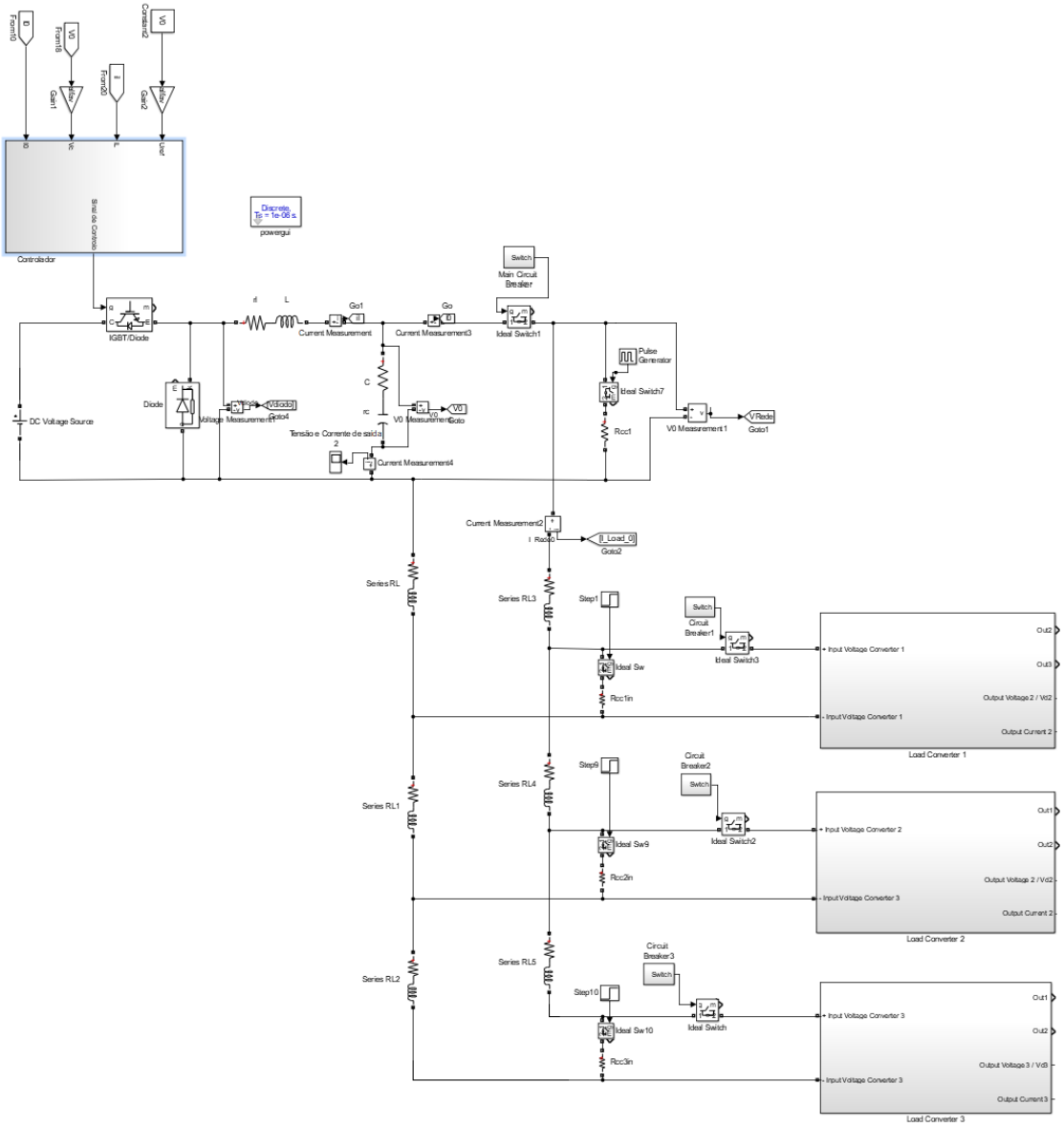

Fig. A.0.1- DC grid mode MATLAB/Simulink

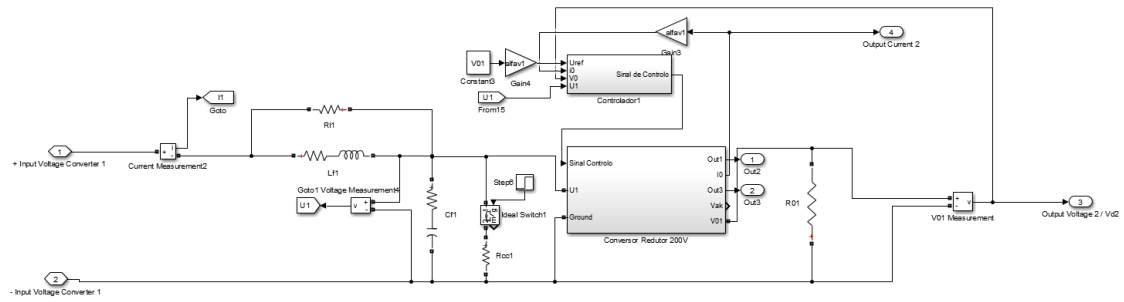

Fig. A.0.2- Constant power load model MATLAB/Simulink